R-04-59

Development and verification of methods to estimate transmissivity distributions and orientation of conductive fractures/features along boreholes

Åsa Fransson, Chalmers tekniska högskola

June 2004

SKB

Development and verification of methods to estimate transmissivity distributions and orientation of conductive fractures/features along boreholes

Åsa Fransson, Chalmers tekniska högskola

June 2004

This report concerns a study which was conducted for SKB. The conclusions and viewpoints presented in the report are those of the author and do not necessarily coincide with those of the client.

A pdf version of this document can be downloaded from www.skb.se

Abstract

Two methods: one non-parametric (M1) and; one based on combinatorics and the multiplication principle (M2), are used to estimate probabilities of conductive/non-conductive fractures and transmissivity distributions. An initial attempt to link inflow and orientation of fractures is also made.

Data to estimate transmissivity distributions originate from Posiva Flow logging of the upper part (206–341 m) of Borehole 2 (KLX02). Estimated transmissivity distributions based on flowlog data from 3 m sections (test scale, L: 3 m, step length, dL: 3 m) are compared to transmissivities obtained from detailed difference flow measurements (test scale, L: 0.5 m, step length, dL: 0.1 m). The agreement is good for both methods, M1 and M2. The study also shows that the method based on combinatorics gives similar distributions when using fractures from core logging and fractures identified in BIPS-images. Data for the inflow-orientation study are inflow during drilling and strike and dip of natural fractures for core borehole KA3367B01. The study shows that most of the fractures from the conductive sections have a NW-direction and a steep dip. According to the stereoplot, none of the fractures found in the sections with the largest inflows are subhorizontal.

What is concluded above indicates that data from fixed-interval-length hydraulic tests and geological mapping of different scales can be utilised and still estimate similar transmissivity distributions of individual features/fractures. Individual fracture transmissivity is useful to estimate hydraulic aperture, which is subsequently used as input information when choosing type of grout and grouting strategy. Information concerning the orientation of conductive fractures is useful when deciding borehole orientation when grouting (e.g. subhorizontal features may demand other borehole directions).

Sammanfattning

Två metoder, en icke-parametrisk (M1) och en vilken baseras på kombinatorik (M2), används för att skatta sannolikheten för vattenförande/täta sprickor och transmissivitetsfördelningar. Dessutom görs ett inledande försök att koppla inflöde och sprickorientering.

Data för att skatta transmissivitetsfördelningar kommer från flödesloggning med Posiva Flow Log i den övre delen (206–341 m) av Borrhål 2 (KLX02). Skattade transmissivitetsfördelningar baseras på flödesloggning i 3 m sektioner (testskala, L: 3 m, steglängd, förflyttning, dL: 3 m) som jämförs med transmissiviteter som är ett resultat av detaljerad flödesloggning (testskala, L: 0.5 m, steglängd, förflyttning, dL: 0.1 m). Överensstämmelsen mellan fördelningarna är god för båda metoderna M1 och M2. Studien visar dessutom att metoden baserad på kombinatorik ger liknande fördelningar med sprickdata ifrån kärnkartering och sprickor som identifierats på BIPS-bilder. Data för studien av inflödeorientering är inflöde under borrning och strykning/stupning för naturliga sprickor längs kärnborrhål KA3367B01. Studien visar att de vattenförande sektionerna har sprickor som är huvudsakligen NV-orienterade och branta. Enligt en stereoplot som sammanställer orientering och inflöde är inga av de sprickor som återfinns i sektioner med de största inflödena subhorisontella.

Det som beskrivs ovan indikerar att data ifrån hydrauliska tester och geologisk kartering med konstant testlängd kan användas för olika testskalor och ändå ge liknande transmissivitetsfördelningar för individuella sprickor. Transmissivitet för enskilda sprickor är användbart för att skatta hydraulisk vidd, vilken kan användas för att bestämma typ av bruk och injekteringsstrategi. Information angående orienteringen hos vattenförande sprickor är av betydelse för att bestämma riktning hos injekteringshål (subhorisontella sprickor kan exempelvis kräva en anpassning).

Contents

1   Introduction

When hydraulically describing fractured rock for grouting, parameters such as hydraulic conductivity or Lugeon values are often used. These parameters do not account for properties of individual features. Since the individual fractures are what need to be sealed to decrease inflow to a tunnel, a description based on fracture properties and not average rock properties seems to be a reasonable choice. The aim of this work is to further develop and verify two methods, which estimate distributions of transmissivity for conductive features/ fractures /Fransson, 2002; Fransson, 2001; Fransson and Rhén, 2002/, see Table 1-1. Transmissivity and estimated hydraulic aperture are useful as guidance to improve grouting strategy. To get a general picture of what has been made to investigate the usefulness of the methods to estimate transmissivity distributions, the aim of earlier publications and this work (in bold) are presented in Table 1-1.

Table 1-1. Transmissivity distributions along boreholes: aim of previous publications and this work.

Paper/publication	Aim
/Fransson, 2002/. Nonparametric method for transmissivity distributions along boreholes. Ground Water, 40(2), 201–204.	**Initial presentation of methods:** The paper presents two methods for estimates of transmissvity and hydraulic aperture distributions along boreholes. Input data are fixed-interval-length transmissivities and corresponding number of fractures for each section.
/Fransson, 2001/. Characterisation of a fractured rock mass for a grouting field test. Tunnelling and Underground Space Technology, 16(4), 331–339.	**Verification for a field test:** The method was used for a grouting field test in a pillar at Äspö HRL /see also Eriksson, 2002/. The result based on the method was in good agreement with what was found during further investigations. This was the case for fracture data originating both from core logging and BIPS-images.Test scale: ~grouting fan
/Fransson and Rhén, 2002/. Estimating probability of conductive fractures using borehole data – A case study. XXXII IAH & ALHSUD Congress, Mar del Plata, Argentina.	**Verification of method:** Case study using data from long, deep boreholes (Laxemar, in the vicinity of Äspö HRL). Are the results obtained from different fixed-interval-lengths similar (3 m and 30 m for KLX01, Laxemar)? Could the result be used for predictions related to another part of the borehole or a borehole in the close vicinity? Answer: Yes. Test scale: ~3 m, 30 m, entire boreholes (KLX01: 1080 m, KLX02: 1700 m)
Development and verification of methods to estimate transmissivity distributions and orientation of conductive fractures/features along boreholes.	**Verification of method: A comparison of transmissivity distributions (based on fixed-interval-length transmissivity and corresponding number of fractures, 3 m sections) and the resulting transmissivity distribution from detailed investigations using Posiva Flow log (using a so called "Sequential flow logging" with section length: 0.5 m and minimum step length: 0.1 m). An initial attempt to link inflow and orientation of fractures is made. Test scale: ~0.5 m, 3 m, (between 206–341 m depth of KLX02: total length 1700 m)**

The main task in this report is to compare estimated transmissivities based on data from fixed-interval-length transmissivity and corresponding number of fractures (3 m sections) to data obtained by detailed difference flow logging (Posiva Flow Log using a so called "Sequential flow logging" with section length: 0.5 m and minimum step length: 0.1 m) to see if the distributions are similar.

To estimate probabilities of conductive/non-conductive fractures and transmissivity distributions, two methods, one non-parametric (M1) and one based on combinatorics and the multiplication principle (M2), were used. Data originate from hydraulic tests and geological mapping along boreholes drilled in crystalline fractured rock at, or in the vicinity of, Äspö Hard Rock Laboratory, on the Southeast coast of Sweden. Finally, an initial study using section inflows and orientation of fractures are made in an attempt to identify the orientation of the most conductive features.

2 Methods

2.1 Transmissivity distributions along boreholes: Non-parametric method, M1

The following assumptions are made for the non-parametric method:

- Hydraulic properties of fractures are statistically independent.

- Fractures act as parallel conduits and are two-dimensional features with cylindrical flow.

- The total borehole transmissivity, T_j, is equal to the sum of the individual fracture transmissivities, $T_j = \sum_{N_j} T_{jk}$.

- For each of all fractures, N, of a section or a borehole, the probability, p/N, of occurring within a given interval [0,p] is the same.

Below, the non-parametric method is briefly presented /see also Fransson, 2002/ and Figure 2-1 shows the two main expressions: $\Theta_N(n/N)_i$ or $\Theta(p)_i$ referred to as the transmissivity distribution and $\tau_N(n/N)_i$ or $\tau(p)_i$ which is the corresponding mean transmissivity function:

$$\tau_N\left(\frac{n}{N}\right)_i = \frac{1}{n}\left(\sum_{m=0}^{n-1}\Theta_N\left(\frac{n}{N}\right)_{im} + \frac{1}{2}\Theta_N\left(\frac{n}{N}\right)_{in}\right) \tag{1}$$

The transmissivities of the N fractures are sorted in ascending order and in a population of e.g. 10 fractures the value of the mean transmissivity function $\tau_N(3/10)_i$ is estimated using the three smallest transmissivities. For $\tau_N(10/10)_i$ all values are used. Going from discrete to continuous expressions, $\tau_N(n/N)_i$ above could also be written:

$$\tau(p_j)_i = \frac{1}{p_j}\int_0^{p_j}\Theta(p)_i\,dp \tag{2}$$

Searching for a population of possible individual transmissivities within a section of a borehole, the mean transmissivity for the borehole section, T_j/N_j, is estimated and assumed to be equal to the mean transmissivity function:

$$\frac{T_j}{N_j} \approx E\langle T_{jk}\rangle = \tau(p_j)_i = \frac{1}{p_j}\int_0^{p_j}\Theta(p)_i\,dp \tag{3}$$
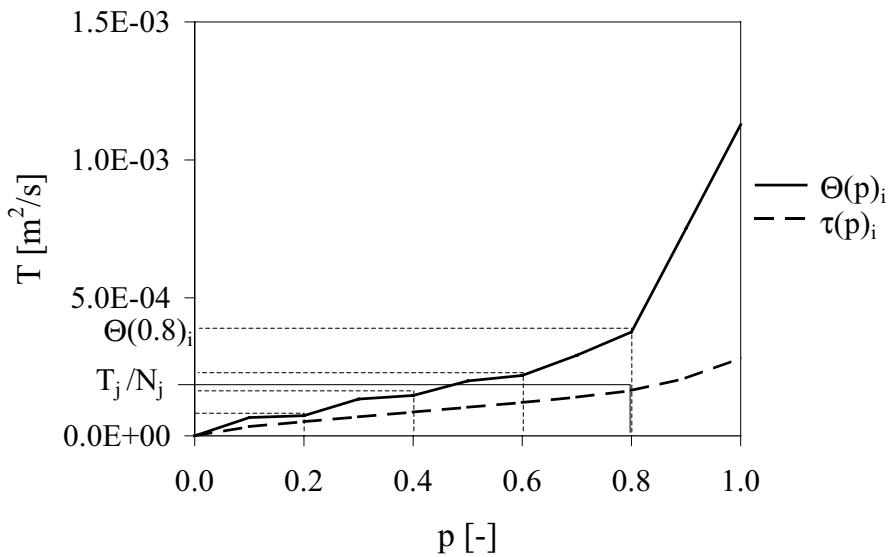
Figure 2-1. *Example where the mean transmissivity for a borehole section, T_j/N_j, is equal to the mean transmissivity function $\tau(p_j)_i$ when $p_j=0.8$, that is, $T_j/N_j = \tau(p_j)_i = \tau(0.8)_i$. The number of fractures, N_j (here 4), would give the transmissivities $\Theta(0.2)_i$, $\Theta(0.4)_i$, $\Theta(0.6)_i$ and $\Theta(0.8)_i$ from the interval [0,0.8] /from Fransson, 2002/.*

In Figure 2-1, the mean transmissivity for the borehole section, T_j/N_j, is equal to the mean transmissivity function $\tau(p_j)_i$ when $p_j=0.8$, that is, $T_j/N_j = \tau(p_j)_i = \tau(0.8)_i$. The number of fractures, N_j (here 4), would give the transmissivities $\Theta(0.2)_i$, $\Theta(0.4)_i$, $\Theta(0.6)_i$ and $\Theta(0.8)_i$ from the interval [0,0.8]. Finally, the transmissivities are sorted in ascending order and evenly distributed within the interval [0,1], resulting in a new transmissivity distribution, $\Theta(p)_{i+1}$. This distribution is then used to estimate the mean transmissivity function $\tau(p)$ for the (i+1)[th] iteration, $\tau(p)_{i+1}$ or $\tau_N(n/N)_{i+1}$; see Equation 2. Calculations according to Equation 3 give new fracture transmissivities as well as a new distribution, $\Theta(p)_{i+2}$, which eventually converges. Since the transmissivity distribution is likely to be skewed, and the trapezoidal rule estimates a value of each transmissivity in the center of the corresponding interval, the total calculated transmissivity of each section, Θ_j, does not necessarily become equal to the measured one, T_j. To get an agreement, the final iteration transmissivities of each section, Θ_j, are adjusted by a factor:

$$F_j = \frac{T_j}{\Theta_j} \qquad (4)$$

The final distribution of transmissivities is not unique (other combinations of transmissivities could exist) but it is in agreement with the number of fractures and the transmissivity of each section. Further, all data originate from the same distribution.

2.2 Transmissivity distributions along boreholes: Method based on combinatorics, M2

For this method as well as for the non-parametric one, hydraulic properties of fractures are assumed to be statistically independent. Further, fractures act as parallel conduits and are two-dimensional features with cylindrical flow. The probability of a section, j, to be tight, p_{tj}, is the result if all intersecting fractures, N_j, are tight, i.e. p_t^{Nj}, see Table 2-1. Based on the section transmissivity, T_j, a section is here defined as tight when the transmissivity is equal to or lower than a measurement limit, T_{lim}, (i.e. the probability of a tight section is 1 if $T_j \leq T_{lim}$). Consequently, a borehole consists of J sections where J_c are conductive and J_t are tight, $J = J_c + J_t$. A correct assumption of the probability of a tight fracture, p_t, should result in an agreement between the probability of a tight section, J_t/J, and the mean of probabilities for a tight section, $\Sigma p_t^{Nj}/J$:

$$\frac{J_t}{J} \approx \frac{\sum_{j=1}^{J} p_t^{N_j}}{J} \tag{5}$$

which gives the approximate probability

$$p_t \approx \frac{J_t}{\sum_{j=1}^{J} p_t^{N_j} \Big/ p_t} \approx \frac{J_t}{\sum_{j=1}^{J} p_t^{N_j-1}} \tag{6}$$

This can be solved by iteration and finally, the probability or frequency of conductive fractures, p_c, is calculated according to:

$$p_c = 1 - p_t \tag{7}$$

A binomial distribution, which is applicable when a fracture is viewed as either tight or conductive, has the mean number of conductive fractures:

$$\mu_c = N \cdot p_c \tag{8}$$

and the standard deviation:

$$\sigma_c = \sqrt{N \cdot p_c (1 - p_c)} \tag{9}$$

Table 2-1. Data for estimating probability of tight and conductive fractures, p_t and p_c, are number of fractures, N_j, and transmissivity, T_j, of each borehole section, j.

Section, j	No of fractures, N_j	Tight, based on T_j, 1 if $T_j \leq T_{lim}$	Tight, estim $p_{tj} = p_t^{Nj}$	Conductive, based on T_j, 1 if $T_j > T_{lim}$	Conductive, estim $p_{cj} = 1-p_t^{Nj}$
1	N_1	0 or 1	p_t^{N1}	1 or 0	$1-pt^{N1}$
2	N_2	0 or 1	p_t^{N2}	1 or 0	$1-pt^{N2}$
...	...	...	...	...	...
j	N_j	0 or 1	p_t^{Nj}	1 or 0	$1-pt^{Nj}$
Σ	N	$\Sigma=J_t$	$p_t^{N1}+p_t^{N2}...$	$\Sigma=J_c$	$(1-p_t^{N1})+(1-p_t^{N2})...$

2.3 Inflow and orientation of conductive features

The objective of this part of the study is to investigate whether inflow during drilling and information concerning the orientation of fractures can be used to identify the orientation of conductive fractures. This information is useful when deciding borehole orientation when grouting (e.g. are there subhorizontal features that demand other borehole directions?). Input data are inflow (or transmissivity) and strike and dip of fractures along a borehole. Data are used to construct a stereoplot.

Inflow and fracture data should be subdivided into sections and Table 2-2 shows how the method based on combinatorics (M2, Table 2-1) for estimating a transmissivity distribution can be utilised as a basis when organising data. The last two columns of Table 2-2 include inflow and a symbol for each section. The same symbol should be used in the stereoplot for all fractures within the same section. Here, the N_1 fractures in Section 1 are assumed to have 0 L/min of inflow and the strike and dip of these fractures should be represented by the symbol X in a stereoplot. The N_2 fractures in Section 2 are assumed to have 10 L/min of inflow and a partly filled circle should in this case represent the strike and dip of the fractures.

Table 2-2. Data for estimating probability of tight and conductive fractures, p_t and p_c, are number of fractures, N_j, and transmissivity, T_j, of each borehole section, j (Table 2-1). To identify orientation of conductive features, inflow and a symbol for each conductive section are added. All fractures within a conductive section are represented by the same symbol in the resulting stereoplot.

Section, j	No of fractures, N_j	Tight, based on T_j, 1 if $T_j \leq T_{lim}$	Tight, estim $p_{tj} = p_t^{Nj}$	Conductive, based on T_j, 1 if $T_j > T_{lim}$	Conductive, estim $p_{cj} = 1-p_t^{Nj}$	Inflow, Q [L/min]	Symbol
1	N_1	0 or 1	p_t^{N1}	1 or 0	$1-p_t^{N1}$	0	⊠
2	N_2	0 or 1	p_t^{N2}	1 or 0	$1-p_t^{N2}$	10	⊕
…	…	…	…	…	…	…	…
j	N_j	0 or 1	p_t^{Nj}	1 or 0	$1-p_t^{Nj}$	Q	⊗
Σ	N	$\Sigma=J_t$	$p_t^{N1}+p_t^{N2}…$	$\Sigma=J_c$	$(1-p_t^{N1})+(1-p_t^{N2})…$		

2.4 Input data

2.4.1 Transmissivity distributions along boreholes

Input data originate from two boreholes (Borehole 1: KLX01 and Borehole 2: KLX02). For both methods (M1: non-parametric and M2: combinatorics) section transmissivity, T_j, and the corresponding number of natural fractures are used to estimate probabilities of conductive fractures and transmissivity distributions. Figure 2-2 and Figure 2-3 show borehole lengths and intervals where hydraulic tests with different packer spacing ("test scale") have been performed /from Fransson and Rhén, 2002/. Test data used for calculations are for Borehole 1 from injection tests in 3- and 30 m sections and for Borehole 2 from flowlogging in 3 m sections. Investigations of the two boreholes are compiled in /Andersson et al, 2002/. The utilised Posiva Flow log /Rouhiainen, 2000/ is based on pulse transit time of a thermal pulse for small flows (0.1–10 mL/min) and thermal dilution rate for high flows (2–500 mL/min).
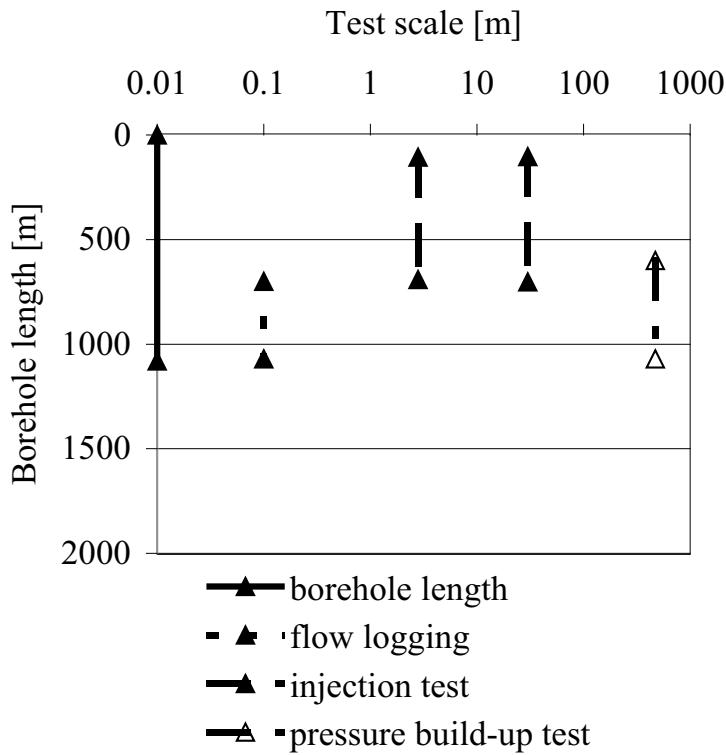
Figure 2-2. *Borehole 1: borehole length and intervals where hydraulic tests with different packer spacing ("test scale") were performed /from Fransson and Rhén, 2002/. Calculations were based on injection tests in 3 m and 30 m sections.*
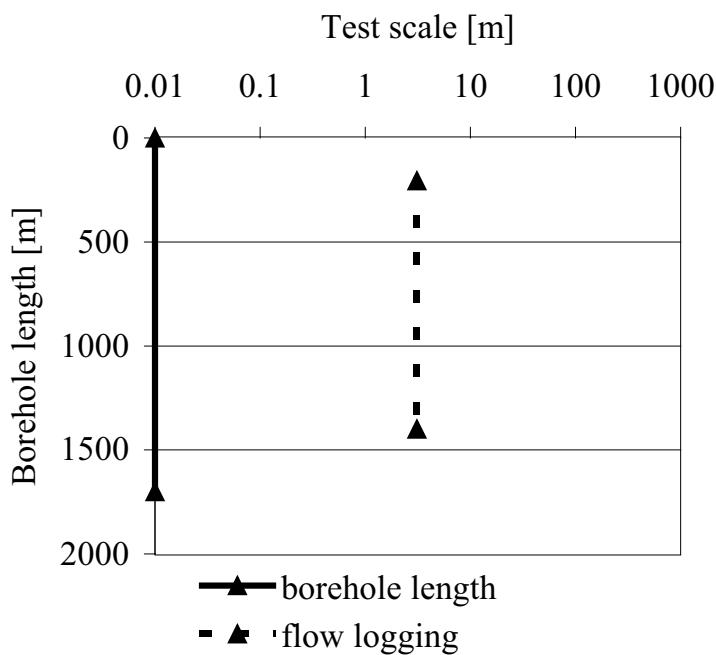
Figure 2-3. *Borehole 2: borehole length and intervals where hydraulic tests with different packer spacing ("test scale") were performed /from Fransson and Rhén, 2002/. Detailed investigations for different test scales (L) and step lengths (dL) were performed in the interval 200–400 m using a difference flow logging method /Ludvigson et al, 2002/. Calculations are based on 3 m section tests (L: 3 m, dL: 3 m).*

The Posiva Flow log method measures changes of flow along the borehole rather than the cumulative flow. The flow rate is measured in a test section (equal to test scale, L) limited by assemblies of soft rubber discs. The test section is moved in steps with step length dL. Data used for calculations have a step length equal to the test scale (3 m). This is referred to as "Sequential flow logging" mode. "Overlapping flow logging" mode aims at determining the exact depth of fractures or fracture zones and the test scale (L) is larger than the step length (dL).

For Borehole 2, results from calculations based on 3 m sections ("Sequential flow logging") should be compared to, detailed investigations ("Overlapping flow logging"). Flow from a fracture is measured as long as the fracture stays within the section. Therefore, the minimum length of a plotted flow anomaly is the section length minus the step length used (in this case 0.4 m since minimum section length is 0.5 m and minimum step length 0.1 m). The flowing fracture is always located at the lower boundary of the anomaly in the plots (by convention). Flowing fractures that are located near each other can be better resolved with a short section length. This is due to the anomalies being overlapped which means that flows from several fractures sums up as long as they stay within the same section. Table 2-3 presents the number of flow anomalies identified for various drawdowns (s), section lengths (L) and step lengths (dL) based on data from /Ludvigson et al, 2002/.

Table 2-3. Number of natural fractures and flow anomalies for different drawdowns (s), section lengths (L) and step lengths (dL) in the interval 200–400 m of Borehole 2, KLX02 (modified from /Ludvigson et al, 2002/).

L(m)/ dL(m)	3/0.5	3/0.5	0.5/0.1	0.5/0.1	0.5/0.1	0.5/0.1	0.5/0.1	0.5/0.1	Core log
Drawdown(m)	s=0	s=8	s=0	s=1	s=2	s=4	s=8	s=22	
Interval(m)				Number of flow anomalies					Total/CZ
200–210	0	0	0	0	0	0	0	0	8
210–220	1	2	4	5	5	5	5	5	26
220–230	2	3	2	5	5	5	5	5	19
230–240	1	3	1	7	7	7	7	7	25/9
240–250	1	3	4	8	8	8	8	8	31
250–260	2	3	4	5	5	5	5	5	34/11
260–270	1	1	2	3	3	3	3	3	29/5
270–280	1	3	1	3	3	4	4	3	10
280–290	0	0	0	0	0	0	0	0	7
290–300	1	3	1	5	5	5	5	5	11
300–310	0	2	0	1	2	2	2	1	7
310–320	1	2	1	2	2	2	3	1	12
320–330	0	2	0	3	4	4	4	0	11
330–340	2	2	4	5	5	5	5	4	29/10
340–350	0	0	0	0	0	0	0	0	6
350–360	0	0	0	0	0	0	0	0	7
360–370	0	0	0	0	0	0	0	0	5
370–380	0	1	0	0	1	1	1	1	3
380–390	0	2	0	1	1	2	2	2	86/60
390–400	0	0	0	0	0	0	0	0	8
Total	13	32	24	53	56	58	59	49	374/95

The number of flow anomalies increases when the section length decreases due to an increased resolution. The drawdown going from 0 to 1 m also increases the number of flow anomalies considerably. Further a decrease is seen for a drawdown of 22 m where some of the flow anomalies are masked due to an increased noise and background flow level. Besides the inflow, single point resistance is also measured and considered an important correlation parameter by the determination of the exact position of flow anomalies. Flow loggings were made downward through the borehole and the single point resistance electrode is found by the upper rubber discs. In this report, data are analysed in the interval 206–341 m. Data for the two boreholes (Borehole 1, KLX01 and Borehole 2, KLX02) are presented in Appendix A.

2.4.2   Inflow and orientation of conductive features

Input data when investigating the relationship between inflow and orientation of conductive features are inflow and strike and dip of natural fractures along the core borehole KA3376B01 (see Appendix B). Inflow originates from measurements during drilling and as a comparison data from difference flow logging are also presented (see Figure B1, Appendix B).

3 Results and discussion

3.1 Transmissivity distributions along boreholes

In /Fransson and Rhén, 2002/, the probabilities of tight and conductive fractures were estimated using the method based on combinatorics (M2, Equations 5–9). Four different assumptions of the measurement limit, $T_{lim}=10^{-9}$, 10^{-8}, 10^{-7} and 10^{-6} m²/s, were made for the calculations and Figure 3-1 presents the results based on data for the hydraulic injection tests performed for 3 m and 30 m sections along Borehole 1 (KLX01, approximately 100–700 m) and for flow logging in 3 m sections (L: 3 m, dL: 3 m) along two different intervals of Borehole 2 (KLX02, 206–701 and 206–1400 m). For the measurement limit, T_{lim}: 10^{-9} m²/s, the probability of a tight fracture, p_t, exceeds 0.9 for data from both 3 m and 30 m sections. Along the tested intervals more than 90% of the fractures is therefore expected to have a transmissivity below $1\cdot10^{-9}$ m²/s.

In this study, data from the upper part (206–341 m) of Borehole 2 (KLX02) were used. The resulting distributions from the non-parametric method (M1, Equations 1–4) and the method based on combinatorics (M2, Equations 5–9) using 3 m-sections ("Sequential flow logging", L: 3 m, dL: 3 m) are compared to results obtained by detailed difference flowlogging (L: 0.5 dL: 0.1, s: 22m, see Appendix A, Table A6).
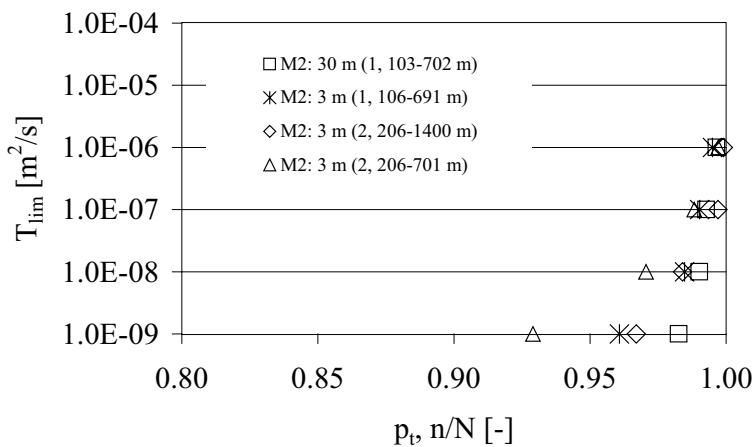
Figure 3-1. *Estimated probabilities of tight fractures, p_t, n/N or $p(T \leq T_{lim})$, for Boreholes 1 and 2 and the measurement limits, $T_{lim}=10^{-9}$, 10^{-8}, 10^{-7} and 10^{-6} m²/s estimated by method based on combinatorics (M2) and data from 3 m and 30 m sections (see Fransson and Rhén, 2002).*

Here as well, four different assumptions of the measurement limit, $T_{lim}=10^{-9}$, 10^{-8}, 10^{-7} and 10^{-6} m²/s, were made for the calculations. Figure 3-2 and Figure 3-3 present the result in two different ways. For Figure 3-2 each triangle, dot or asterisk represents one fracture (total number of natural fractures, N: 256, see Table 3-1). For Figure 3-3 the same data are used to show the resulting number of conductive fractures for the intervals 10^{-8}–10^{-7}, 10^{-7}–10^{-6} and 10^{-6}–10^{-5} m²/s. The method based on combinatorics (M2) results in a distribution for all fractures without considering location, whereas the non-parametric method (M1) gives estimates of transmissivities for the fractures within each section. For the transmissivities identified by detailed flow logging and the result based on the method M2, data are sorted in ascending order. For method M1, the probabilities of tight features, p_t, are estimated directly based on Equations 5–9.

For data identified by detailed difference flow logging, L: 0.5 m, dL: 0.1 m (asterisk), 10% of the fractures have a transmissivity larger than $1\cdot10^{-8}$ m²/s (90% smaller, see Figure 3-2). For the method based on combinatorics (M2) approximately the same result is obtained since a transmissivity larger than $1\cdot10^{-8}$ m²/s corresponds to the probability of a conductive fracture, p_c, of 10% (p_t, of 90%, see Figure 3-2). This results in a mean number of conductive fractures, μ_c (Equation 8), with a transmissivity above $1\cdot10^{-8}$ m²/s to be 26 (equals the number of dots found above $1\cdot10^{-8}$ m²/s). Also for the results for the non-parametric method the general agreement is good, with minor deviations for the largest and the smaller transmissivities. One reason for the difference between the result from data identified by detailed difference flow logging and data for the two methods is that the summation of transmissivities for the two data sets (individual fractures and 3 m sections) is not exactly the same. The main difference is seen for the section where the largest transmissivity is found.
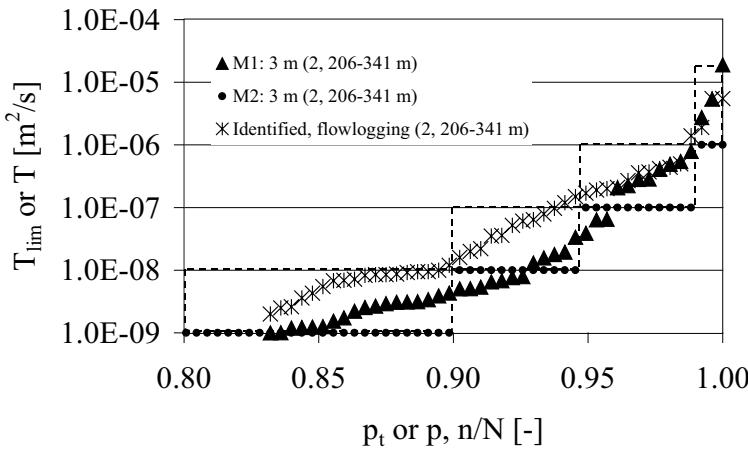
Figure 3-2. *Estimated probabilities of tight fractures, p_t, n/N or $p(T \leq T_{lim})$, for the measurement limits, $T_{lim}=10^{-9}$, 10^{-8}, 10^{-7} and 10^{-6} m²/s based on the two methods (M1: non-parametric and M2: combinatorics) and data from 3 m sections (L: 3m, dL: 3m). Data are compared to features identified by detailed flowlogging. Each dot represents one of the 256 fractures.*
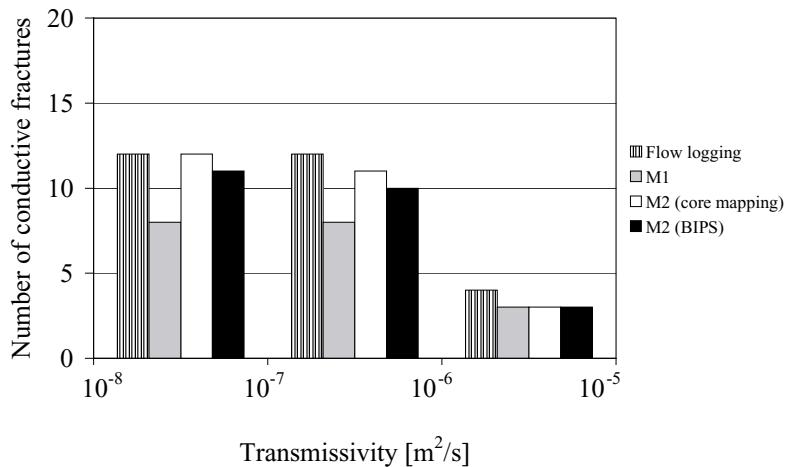
Figure 3-3. *Number of conductive fractures for intervals 10^{-8}–10^{-7}, 10^{-7}–10^{-6} and 10^{-6}–10^{-5} m²/s identified by detailed difference flow logging compared to estimated number of fractures using non-parametric method (M1) and based on combinatorics (M2). Data originate from Table 3-1 and are also presented in Figure 3-2.*

Table 3-1 also presents estimated probabilities and number of conductive, non-conductive fractures based on combinatorics (M2) and the number of fractures originating from all interpreted structures from BIPS-images /Carlsten et al, 2001/. The agreement between results obtained using number of fractures from core mapping and from BIPS-images is good. This was also the result in /Fransson, 2001/ where fractures in a pillar were investigated using hydraulic tests and geological mapping for a 9-meter long borehole.

Table 3-1. Fractures identified by detailed difference flow logging compared to: a) estimated number of fractures exceeding the transmissivities 10^{-6}, 10^{-7} and 10^{-8} m²/s using non-parametric (M1) and; b) estimated probabilities and number of conductive, non-conductive fractures based on combinatorics (M2). Number of fractures originates from core logging (256) and BIPS-images (154).

Flow logging	M1	M2 (N: 256 fractures, from core logging)				M2 (N: 154 fractures, from BIPS-images)			
No of fractures		p_t	p_c	μ_c	σ_c	p_t	p_c	μ_c	σ_c
$T>10^{-6}$		T_{lim}:10^{-6}				T_{lim}:10^{-6}			
4	**3**	0.99	0.01	**3**	2	0.98	0.02	**3**	2
$T>10^{-7}$		T_{lim}:10^{-7}				T_{lim}:10^{-7}			
16	**11**	0.95	0.05	**14**	4	0.92	0.08	**13**	3
$T>10^{-8}$		T_{lim}:10^{-8}				T_{lim}:10^{-8}			
28	**19**	0.90	0.30	**26**	5	0.84	0.16	**24**	4

3.2   Inflow and orientation of conductive features

Data describing inflow measured during drilling and strike and dip of fractures along the borehole KA3376B01 were subdivided into 3 m sections (Appendix B). Five sections were found to have larger inflows (5–49 L/min) and Figure 3-4 presents these inflows and what symbols that were used. The orientations of fractures for the different symbols (inflows) are compiled in the stereoplot.
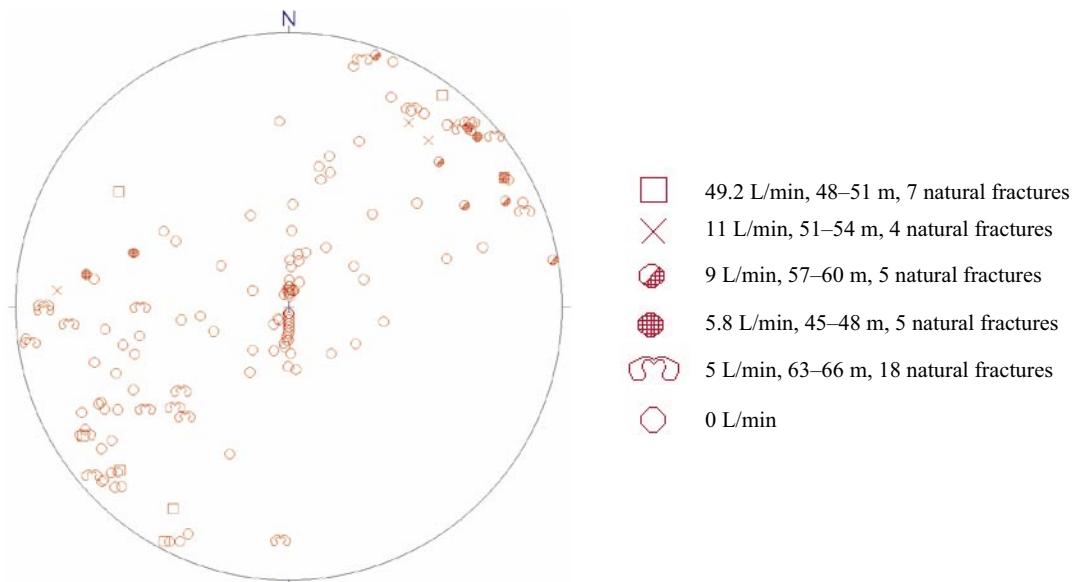
Figure 3-4. *Stereoplot for natural fractures along core borehole KA3376B01. Symbols describe fractures originating from sections (3 m) with different inflows.*

Most of the fractures from the conductive sections (identified by a square) have a NW-direction and a steep dip. According to the stereoplot, none of the fractures found in the sections with the largest inflows are subhorizontal.

4 Conclusions

This study aims at developing and verifying the usefulness of two methods, one non-parametric (M1) and one based on combinatorics (M2), which estimate the probability of conductive fractures/features along a borehole. Further, the second method (M2) in combination with the use of stereoplots is utilised to identify how inflow and the orientation of fractures are related. Data when investigating the probability of conductive fractures originate from two long, vertical boreholes (KLX01: Borehole 1 and KLX02: Borehole 2) drilled in crystalline bedrock in the vicinity of Äspö Hard Rock Laboratory situated in the Southeast of Sweden. The inflow-orientation study is based on measurements of inflow during drilling and strike and dip of fractures along core borehole KA3376B01 at Äspö Hard Rock Laboratory.

An earlier study /Fransson and Rhén, 2002/ shows that the method based on combinatorics (M2) gives a good agreement when comparing the probability of tight/conductive fractures for different section lengths (3- and 30 meter sections). This indicates that hydraulic tests of different section lengths, together with mapping of the core, can be utilized and still estimate similar probabilities of conductive fractures and distributions of transmissivity. According to calculations, only a few of the fractures had high transmissivities, which is in agreement with the skew transmissivity distributions that are commonly found in fractured rock.

In this study, data from the upper part (206–341 m) of Borehole 2 (KLX02) were used. The resulting distributions from the non-parametric method and the method based on combinatorics using data from 3m sections (test scale, L: 3 m, step length, dL: 3 m) are compared to results obtained by detailed difference flow measurements (test scale, L: 0.5 m, step length, dL: 0.1 m). The agreement is good for both methods. The non-parametric method gives estimates of transmissivities for the fractures within each section, whereas the method based on combinatorics results in a distribution for all fractures without considering location along borehole. The study also shows that the method based on combinatorics (M2) gives similar results when using fractures from core logging and fractures identified in BIPS-images. This is in agreement with the results in /Fransson, 2001/ where core logging and BIPS data were used for a 9-meter long borehole.

For core borehole KA3376B01, the inflow-orientation study indicates that most of the fractures from the conductive sections have a NW-direction and a steep dip. According to the stereoplot, none of the fractures found in the sections with the largest inflows are subhorizontal. This information is useful when deciding borehole orientation when grouting (e.g. are there subhorizontal features that demand other borehole directions?).

What is concluded above indicates that data from hydraulic tests and geological mapping at different scales can be utilised and still describe similar transmissivity distributions of individual features/fractures. Individual fracture transmissivity is useful to estimate hydraulic aperture, which is subsequently used as input information when choosing type of grout and grouting strategy.

5   References

Andersson J, Berglund B, Follin S, Hakami E, Halvorson J, Hermanson J, Laaksoharju M, Rhén I, Wahlgren C-H, 2002. Testing the methodology for site descriptive modelling Application for the Laxemar area. SKB Report TR-02-19. Svensk Kärnbränslehantering AB.

Carlsten S, Stråhle A , Ludvigson J-E, 2001. Conductive fracture mapping. A study on the correlation between borehole TV- and radar images and difference flow logging results in borehole KLX02. SKB Report R-01-48. Svensk Kärnbränslehantering AB.

Eriksson M, 2002. Grouting field experiment at the Äspö Hard Rock Laboratory, Tunnelling and Underground Space Technology, Volume 17, No. 3, pp 287–293.

Fransson Å, 2001. Characterisation of a fractured rock mass for a grouting field test. Tunnelling and Underground Space Technology, Volume 16, No. 4, pp 331–339.

Fransson Å, 2002. Nonparametric method for transmissivity distributions along boreholes. Ground Water, 40(2), pp 201–204.

Fransson Å, Rhén I, 2002. Estimating probability of conductive fractures using borehole data – A case study. XXXII IAH & ALHSUD Congress, Mar del Plata, Argentina.

Ludvigson J-E, Hansson K , Rouhiainen P, 2002. Methodology study of Posiva difference flow meter in borehole KLX02 at Laxemar. SKB Report R-01-52. Svensk Kärnbränslehantering AB.

Rouhiainen P, 2000. Difference flow measurements in borehole KLX02 at Laxemar. Äspö Hard Rock Laboratory. SKB IPR 01-06. Svensk Kärnbränslehantering AB.

Data for Borehole 1: KLX01 and Borehole 2: KLX02 for estimates of transmissivity distributions along boreholes

Table A1. Transmissivity data from injection tests, test scale (L) 30 m, 103-702 m.

Borehole	Sec up (m)	Sec low (m)	T (m2/s)
KLX01	103.00	133.00	2.6E-08
KLX01	133.00	163.00	2.1E-09
KLX01	163.00	193.00	3.3E-05
KLX01	193.00	223.00	1.6E-07
KLX01	223.00	253.00	1.9E-10
KLX01	253.00	283.00	4.2E-06
KLX01	283.00	313.00	2.5E-07
KLX01	313.00	343.00	8.1E-09
KLX01	343.00	373.00	1.9E-10
KLX01	373.00	403.00	2.3E-09
KLX01	403.00	433.00	2.1E-06
KLX01	433.00	463.00	5.1E-05
KLX01	463.00	493.00	2.0E-10
KLX01	493.00	523.00	3.9E-09
KLX01	523.00	553.00	2.5E-10
KLX01	553.00	583.00	2.1E-10
KLX01	583.00	613.00	3.3E-08
KLX01	613.00	643.00	3.9E-07
KLX01	643.00	673.00	3.0E-07
KLX01	673.00	702.11	1.9E-06

Table A2. Transmissivity data from injection tests, test scale (L) 3 m, 106-691 m.

Borehole	Sec up (m)	Sec low (m)	T (m2/s)	Borehole	Sec up (m)	Sec low (m)	T (m2/s)	Borehole	Sec up (m)	Sec low (m)	T (m2/s)
KLX01	106.00	109.00	4.4E-10	KLX01	295.00	298.00	1.1E-10	KLX01	493.00	496.00	4.9E-10
KLX01	109.00	112.00	2.6E-08	KLX01	298.00	301.00	8.7E-07	KLX01	496.00	499.00	1.2E-10
KLX01	112.00	115.00	1.1E-09	KLX01	301.00	304.00	1.5E-08	KLX01	499.00	502.00	2.6E-10
KLX01	115.00	118.00	5.4E-10	KLX01	304.00	307.00	9.9E-09	KLX01	502.00	505.00	8.7E-10
KLX01	118.00	121.00	6.1E-10	KLX01	307.00	310.00	8.9E-10	KLX01	505.00	508.00	1.2E-09
KLX01	121.00	124.00	5.7E-11	KLX01	310.00	313.00	1.0E-09	KLX01	508.00	511.00	4.8E-10
KLX01	124.00	127.00	1.6E-10	KLX01	313.00	316.00	3.5E-10	KLX01	511.00	514.00	7.5E-09
KLX01	127.00	130.00	2.1E-09	KLX01	316.00	319.00	3.3E-10	KLX01	514.00	517.00	1.2E-09
KLX01	130.00	133.00	9.3E-10	KLX01	319.00	322.00	2.9E-10	KLX01	517.00	520.00	9.9E-11
KLX01	133.00	136.00	2.6E-10	KLX01	322.00	325.00	2.2E-10	KLX01	520.00	523.00	1.6E-09
KLX01	136.00	139.00	4.2E-10	KLX01	325.00	328.00	3.3E-11	KLX01	523.00	526.00	1.9E-10
KLX01	139.00	142.00	2.9E-09	KLX01	328.00	331.00	3.5E-10	KLX01	526.00	529.00	5.1E-10
KLX01	142.00	145.00	2.6E-10	KLX01	331.00	334.00	1.3E-08	KLX01	529.00	532.00	3.0E-10
KLX01	145.00	148.00	3.5E-10	KLX01	334.00	337.00	8.7E-10	KLX01	532.00	535.00	3.3E-10
KLX01	148.00	151.00	2.9E-10	KLX01	337.00	340.00	5.1E-10	KLX01	535.00	538.00	2.8E-09
KLX01	151.00	154.00	3.3E-10	KLX01	340.00	343.00	1.1E-09	KLX01	538.00	541.00	2.8E-09
KLX01	154.00	157.00	1.2E-10	KLX01	343.00	346.00	7.2E-10	KLX01	541.00	544.00	1.0E-09
KLX01	156.00	159.00	5.4E-11	KLX01	346.00	349.00	3.2E-10	KLX01	544.00	547.00	2.4E-10
KLX01	159.00	162.00	2.8E-09	KLX01	349.00	352.00	4.8E-10	KLX01	547.00	550.00	6.3E-10
KLX01	162.00	165.00	1.6E-09	KLX01	352.00	355.00	7.0E-10	KLX01	550.00	553.00	3.3E-10
KLX01	163.00	166.00	8.7E-10	KLX01	355.00	358.00	6.2E-10	KLX01	553.00	556.00	4.5E-09
KLX01	165.00	168.00	1.4E-09	KLX01	358.00	361.00	2.9E-10	KLX01	556.00	559.00	7.2E-10
KLX01	166.00	169.00	8.1E-10	KLX01	361.00	364.00	6.9E-10	KLX01	559.00	562.00	6.3E-10
KLX01	169.00	172.00	1.1E-09	KLX01	364.00	367.00	3.1E-10	KLX01	562.00	565.00	2.4E-10
KLX01	172.00	175.00	1.3E-10	KLX01	367.00	370.00	9.3E-10	KLX01	565.00	568.00	6.9E-10
KLX01	175.00	178.00	2.5E-08	KLX01	370.00	373.00	2.5E-10	KLX01	568.00	571.00	2.3E-09
KLX01	178.00	181.00	7.2E-09	KLX01	373.00	376.00	2.2E-10	KLX01	571.00	574.00	3.3E-10
KLX01	181.00	184.00	3.3E-05	KLX01	376.00	379.00	3.1E-10	KLX01	574.00	577.00	3.6E-09
KLX01	184.00	187.00	3.3E-06	KLX01	379.00	382.00	1.5E-10	KLX01	577.00	580.00	2.2E-11
KLX01	187.00	190.00	4.8E-11	KLX01	382.00	385.00	5.7E-09	KLX01	580.00	583.00	1.9E-09
KLX01	190.00	193.00	1.4E-10	KLX01	385.00	388.00	3.2E-10	KLX01	583.00	586.00	4.2E-10
KLX01	193.00	196.00	1.4E-09	KLX01	388.00	391.00	2.4E-10	KLX01	586.00	589.00	1.6E-09
KLX01	196.00	199.00	1.0E-09	KLX01	391.00	394.00	2.9E-10	KLX01	589.00	592.00	1.5E-08
KLX01	199.00	202.00	3.7E-10	KLX01	394.00	397.00	4.8E-08	KLX01	592.00	595.00	2.7E-09
KLX01	202.00	205.00	9.3E-09	KLX01	397.00	400.00	2.5E-10	KLX01	595.00	598.00	1.6E-09
KLX01	205.00	208.00	2.6E-10	KLX01	400.00	403.00	5.6E-10	KLX01	598.00	601.00	1.2E-10
KLX01	208.00	211.00	5.4E-11	KLX01	403.00	406.00	1.2E-10	KLX01	601.00	604.00	4.8E-09
KLX01	211.00	214.00	1.2E-06	KLX01	406.00	409.00	3.7E-09	KLX01	604.00	607.00	5.1E-10
KLX01	214.00	217.00	2.7E-11	KLX01	409.00	412.00	1.7E-07	KLX01	607.00	610.00	5.4E-09
KLX01	217.00	220.00	1.2E-09	KLX01	412.00	415.00	1.5E-08	KLX01	610.00	613.00	3.8E-10
KLX01	220.00	223.00	3.0E-09	KLX01	415.00	418.00	6.5E-10	KLX01	613.00	616.00	2.2E-09
KLX01	223.00	226.00	2.6E-11	KLX01	418.00	421.00	9.6E-10	KLX01	616.00	619.00	1.2E-09
KLX01	226.00	229.00	6.0E-10	KLX01	421.00	424.00	5.1E-07	KLX01	619.00	622.00	1.6E-10
KLX01	229.00	232.00	1.4E-10	KLX01	424.00	427.00	4.5E-10	KLX01	622.00	625.00	2.2E-09
KLX01	229.00	232.00	8.7E-10	KLX01	427.00	430.00	1.1E-10	KLX01	625.00	628.00	1.8E-09
KLX01	232.00	235.00	5.0E-10	KLX01	430.00	433.00	2.3E-11	KLX01	628.00	631.00	3.9E-10
KLX01	235.00	238.00	4.0E-10	KLX01	433.00	436.00	5.4E-11	KLX01	631.00	634.00	3.3E-07
KLX01	238.00	241.00	1.4E-09	KLX01	436.00	439.00	5.4E-10	KLX01	634.00	637.00	3.3E-07
KLX01	241.00	244.00	7.5E-11	KLX01	439.00	442.00	1.0E-10	KLX01	637.00	640.00	3.6E-07
KLX01	244.00	247.00	2.2E-09	KLX01	442.00	445.00	2.9E-10	KLX01	640.00	643.00	9.9E-10
KLX01	247.00	250.00	1.8E-10	KLX01	445.00	448.00	5.4E-11	KLX01	643.00	646.00	8.3E-09
KLX01	250.00	253.00	6.1E-10	KLX01	448.00	451.00	1.4E-10	KLX01	646.00	649.00	3.0E-10
KLX01	253.00	256.00	3.9E-10	KLX01	451.00	454.00	9.6E-09	KLX01	649.00	652.00	1.4E-09
KLX01	256.00	259.00	2.1E-10	KLX01	454.00	457.00	9.3E-11	KLX01	652.00	655.00	2.7E-09
KLX01	259.00	262.00	7.0E-10	KLX01	457.00	460.00	1.6E-05	KLX01	655.00	658.00	8.0E-09
KLX01	262.00	265.00	2.8E-10	KLX01	460.00	463.00	2.3E-05	KLX01	658.00	661.00	2.4E-10
KLX01	265.00	268.00	1.1E-10	KLX01	463.00	466.00	4.0E-10	KLX01	661.00	664.00	8.4E-10
KLX01	268.00	271.00	5.8E-10	KLX01	466.00	469.00	2.3E-10	KLX01	664.00	667.00	4.4E-10
KLX01	271.00	274.00	3.1E-10	KLX01	469.00	472.00	1.7E-10	KLX01	667.00	670.00	1.0E-09
KLX01	274.00	277.00	9.6E-06	KLX01	472.00	475.00	1.4E-10	KLX01	670.00	673.00	1.3E-07
KLX01	277.00	280.00	6.2E-10	KLX01	475.00	478.00	2.0E-10	KLX01	673.00	676.00	2.7E-09
KLX01	280.00	283.00	1.9E-10	KLX01	478.00	481.00	1.1E-10	KLX01	676.00	679.00	9.3E-10
KLX01	283.00	286.00	1.2E-10	KLX01	481.00	484.00	6.8E-11	KLX01	679.00	682.00	4.2E-09
KLX01	286.00	289.00	7.4E-10	KLX01	484.00	487.00	3.5E-11	KLX01	682.00	685.00	1.9E-09
KLX01	289.00	292.00	1.4E-06	KLX01	487.00	490.00	1.8E-10	KLX01	685.00	688.00	2.2E-08
KLX01	292.00	295.00	1.3E-10	KLX01	490.00	493.00	4.5E-10	KLX01	688.00	691.00	1.6E-06

Table A3. Number of natural fractures (last columns, includes natural_sum and crush_sum) for 3 and 30 meter between approximately 103-702 m for KLX01.

IDCODE	FROM_LENGTH	TO_LENGTH	BHLENGTH	3m		IDCODE	FROM_LENGTH	TO_LENGTH	BHLENGTH	30m
KLX01	106	109	108.5	4		KLX01	103	133	132.5	76
KLX01	109	112	111.5	6		KLX01	133	163	162.5	108
KLX01	112	115	114.5	10		KLX01	163	193	192.5	98
KLX01	115	118	117.5	8		KLX01	193	223	222.5	106
KLX01	118	121	120.5	5		KLX01	223	253	252.5	95
KLX01	121	124	123.5	16		KLX01	253	283	282.5	78
KLX01	124	127	126.5	9		KLX01	283	313	312.5	67
KLX01	127	130	129.5	6		KLX01	313	343	342.5	82
KLX01	130	133	132.5	10		KLX01	343	373	372.5	60
KLX01	133	136	135.5	8		KLX01	373	403	402.5	65
KLX01	136	139	138.5	7		KLX01	403	433	432.5	99
KLX01	139	142	141.5	5		KLX01	433	463	462.5	100
KLX01	142	145	144.5	5		KLX01	463	493	492.5	72
KLX01	145	148	147.5	3		KLX01	493	523	522.5	58
KLX01	148	151	150.5	3		KLX01	523	553	552.5	66
KLX01	151	154	153.5	9		KLX01	553	583	582.5	60
KLX01	154	157	156.5	4		KLX01	583	613	612.5	141
KLX01	157	160	159.5	25		KLX01	613	643	642.5	132
KLX01	160	163	162.5	39		KLX01	643	673	672.5	37
KLX01	163	166	165.5	13		KLX01	673	702	701.5	83
KLX01	166	169	168.5	13						1683
KLX01	169	172	171.5	3						
KLX01	172	175	174.5	7						
KLX01	175	178	177.5	7						
KLX01	178	181	180.5	2						
KLX01	181	184	183.5	23						
KLX01	184	187	186.5	12						
KLX01	187	190	189.5	12						
KLX01	190	193	192.5	6						
KLX01	193	196	195.5	8						
KLX01	196	199	198.5	6						
KLX01	199	202	201.5	4						
KLX01	202	205	204.5	10						
KLX01	205	208	207.5	6						
KLX01	208	211	210.5	12						
KLX01	211	214	213.5	17						
KLX01	214	217	216.5	6						
KLX01	217	220	219.5	8						
KLX01	220	223	222.5	29						
KLX01	223	226	225.5	8						
KLX01	226	229	228.5	5						
KLX01	229	232	231.5	11						
KLX01	232	235	234.5	10						
KLX01	235	238	237.5	14						
KLX01	238	241	240.5	10						
KLX01	241	244	243.5	13						
KLX01	244	247	246.5	12						
KLX01	247	250	249.5	5						
KLX01	250	253	252.5	7						
KLX01	253	256	255.5	12						
KLX01	256	259	258.5	7						
KLX01	259	262	261.5	10						
KLX01	262	265	264.5	11						
KLX01	265	268	267.5	8						
KLX01	268	271	270.5	4						
KLX01	271	274	273.5	7						
KLX01	274	277	276.5	4						
KLX01	277	280	279.5	9						
KLX01	280	283	282.5	6						
KLX01	283	286	285.5	4						
KLX01	286	289	288.5	8						
KLX01	289	292	291.5	6						
KLX01	292	295	294.5	5						
KLX01	295	298	297.5	4						
KLX01	298	301	300.5	7						
KLX01	301	304	303.5	9						
KLX01	304	307	306.5	10						
KLX01	307	310	309.5	4						
KLX01	310	313	312.5	10						
KLX01	313	316	315.5	6						
KLX01	316	319	318.5	7						
KLX01	319	322	321.5	5						
KLX01	322	325	324.5	5						
KLX01	325	328	327.5	17						

IDCODE	FROM_LENGTH	TO_LENGTH	BHLENGTH	3m
KLX01	328	331	330.5	10
KLX01	331	334	333.5	6
KLX01	334	337	336.5	11
KLX01	337	340	339.5	10
KLX01	340	343	342.5	5
KLX01	343	346	345.5	2
KLX01	346	349	348.5	3
KLX01	349	352	351.5	3
KLX01	352	355	354.5	1
KLX01	355	358	357.5	7
KLX01	358	361	360.5	9
KLX01	361	364	363.5	5
KLX01	364	367	366.5	12
KLX01	367	370	369.5	13
KLX01	370	373	372.5	5
KLX01	373	376	375.5	4
KLX01	376	379	378.5	8
KLX01	379	382	381.5	17
KLX01	382	385	384.5	13
KLX01	385	388	387.5	5
KLX01	388	391	390.5	6
KLX01	391	394	393.5	2
KLX01	394	397	396.5	5
KLX01	397	400	399.5	1
KLX01	400	403	402.5	4
KLX01	403	406	405.5	10
KLX01	406	409	408.5	6
KLX01	409	412	411.5	7
KLX01	412	415	414.5	7
KLX01	415	418	417.5	6
KLX01	418	421	420.5	24
KLX01	421	424	423.5	2
KLX01	424	427	426.5	6
KLX01	427	430	429.5	22
KLX01	430	433	432.5	9
KLX01	433	436	435.5	11
KLX01	436	439	438.5	11
KLX01	439	442	441.5	15
KLX01	442	445	444.5	6
KLX01	445	448	447.5	9
KLX01	448	451	450.5	1
KLX01	451	454	453.5	2
KLX01	454	457	456.5	7
KLX01	457	460	459.5	26
KLX01	460	463	462.5	12
KLX01	463	466	465.5	16
KLX01	466	469	468.5	3
KLX01	469	472	471.5	8
KLX01	472	475	474.5	2
KLX01	475	478	477.5	4
KLX01	478	481	480.5	2
KLX01	481	484	483.5	8
KLX01	484	487	486.5	6
KLX01	487	490	489.5	4
KLX01	490	493	492.5	19
KLX01	493	496	495.5	3
KLX01	496	499	498.5	1
KLX01	499	502	501.5	6
KLX01	502	505	504.5	3
KLX01	505	508	507.5	4
KLX01	508	511	510.5	3
KLX01	511	514	513.5	14
KLX01	514	517	516.5	4
KLX01	517	520	519.5	11
KLX01	520	523	522.5	9
KLX01	523	526	525.5	6
KLX01	526	529	528.5	2
KLX01	529	532	531.5	12
KLX01	532	535	534.5	12
KLX01	535	538	537.5	11
KLX01	538	541	540.5	4
KLX01	541	544	543.5	5
KLX01	544	547	546.5	7
KLX01	547	550	549.5	4
KLX01	550	553	552.5	3

IDCODE	FROM_LENGTH	TO_LENGTH	BHLENGTH	3m
KLX01	553	556	555.5	6
KLX01	556	559	558.5	11
KLX01	559	562	561.5	7
KLX01	562	565	564.5	4
KLX01	565	568	567.5	6
KLX01	568	571	570.5	12
KLX01	571	574	573.5	2
KLX01	574	577	576.5	3
KLX01	577	580	579.5	6
KLX01	580	583	582.5	3
KLX01	583	586	585.5	6
KLX01	586	589	588.5	26
KLX01	589	592	591.5	18
KLX01	592	595	594.5	16
KLX01	595	598	597.5	11
KLX01	598	601	600.5	15
KLX01	601	604	603.5	23
KLX01	604	607	606.5	15
KLX01	607	610	609.5	6
KLX01	610	613	612.5	5
KLX01	613	616	615.5	7
KLX01	616	619	618.5	20
KLX01	619	622	621.5	5
KLX01	622	625	624.5	16
KLX01	625	628	627.5	4
KLX01	628	631	630.5	14
KLX01	631	634	633.5	20
KLX01	634	637	636.5	25
KLX01	637	640	639.5	20
KLX01	640	643	642.5	1
KLX01	643	646	645.5	2
KLX01	646	649	648.5	2
KLX01	649	652	651.5	0
KLX01	652	655	654.5	3
KLX01	655	658	657.5	4
KLX01	658	661	660.5	4
KLX01	661	664	663.5	5
KLX01	664	667	666.5	5
KLX01	667	670	669.5	8
KLX01	670	673	672.5	4
KLX01	673	676	675.5	2
KLX01	676	679	678.5	2
KLX01	679	682	681.5	9
KLX01	682	685	684.5	8
KLX01	685	688	687.5	11
KLX01	688	691	690.5	7

Table A4. Transmissivity based on Posiva Flowlogg, test scale (L) 3 m, step length (dL) 3 m, approximately 206-341 m (measurements performed in the interval 206-1400 m, /Ludvigson et al, 2002/).

Borehole	Depth	Secup	Seclow	Scale	K	K*3
KLX02	207.42	205.92	208.92	3	1.05E-09	3.15E-09
KLX02	210.42	208.92	211.92	3	2.64E-09	7.92E-09
KLX02	213.42	211.92	214.92	3	9.11E-07	2.73E-06
KLX02	216.42	214.92	217.92	3	2.13E-08	6.39E-08
KLX02	219.42	217.92	220.92	3	2.34E-09	7.02E-09
KLX02	222.42	220.92	223.92	3	9.54E-10	2.86E-09
KLX02	225.42	223.92	226.92	3	9.51E-08	2.85E-07
KLX02	228.42	226.92	229.92	3	1.36E-07	4.08E-07
KLX02	231.42	229.92	232.92	3	2.93E-09	8.79E-09
KLX02	234.42	232.92	235.92	3	1.12E-08	3.36E-08
KLX02	237.42	235.92	238.92	3	1.52E-09	4.56E-09
KLX02	240.42	238.92	241.92	3	5.95E-09	1.79E-08
KLX02	243.42	241.92	244.92	3	5.69E-09	1.71E-08
KLX02	246.42	244.92	247.92	3	6.92E-08	2.08E-07
KLX02	249.42	247.92	250.92	3	9.42E-08	2.83E-07
KLX02	252.42	250.92	253.92	3	6.35E-06	1.91E-05
KLX02	255.42	253.92	256.92	3	4.07E-09	1.22E-08
KLX02	258.42	256.92	259.92	3	9.90E-12	2.97E-11
KLX02	261.42	259.92	262.92	3	9.90E-12	2.97E-11
KLX02	264.42	262.92	265.92	3	9.90E-12	2.97E-11
KLX02	267.42	265.92	268.92	3	7.58E-08	2.27E-07
KLX02	270.42	268.92	271.92	3	1.82E-07	5.46E-07
KLX02	273.42	271.92	274.92	3	2.27E-09	6.81E-09
KLX02	276.42	274.92	277.92	3	1.70E-09	5.10E-09
KLX02	279.42	277.92	280.92	3	9.90E-12	2.97E-11
KLX02	282.42	280.92	283.92	3	9.90E-12	2.97E-11
KLX02	285.42	283.92	286.92	3	9.90E-12	2.97E-11
KLX02	288.42	286.92	289.92	3	2.68E-10	8.04E-10
KLX02	291.42	289.92	292.92	3	4.34E-09	1.30E-08
KLX02	294.42	292.92	295.92	3	1.64E-07	4.92E-07
KLX02	297.42	295.92	298.92	3	2.17E-08	6.51E-08
KLX02	300.42	298.92	301.92	3	2.54E-09	7.62E-09
KLX02	303.42	301.92	304.92	3	9.90E-12	2.97E-11
KLX02	306.42	304.92	307.92	3	1.50E-10	4.50E-10
KLX02	309.42	307.92	310.92	3	1.11E-09	3.33E-09
KLX02	312.42	310.92	313.92	3	9.97E-11	2.99E-10
KLX02	315.42	313.92	316.92	3	4.55E-10	1.37E-09
KLX02	318.42	316.92	319.92	3	1.80E-06	5.40E-06
KLX02	321.42	319.92	322.92	3	9.90E-12	2.97E-11
KLX02	324.42	322.92	325.92	3	7.60E-10	2.28E-09
KLX02	327.42	325.92	328.92	3	1.89E-09	5.67E-09
KLX02	330.42	328.92	331.92	3	1.04E-09	3.12E-09
KLX02	333.42	331.92	334.92	3	2.61E-10	7.83E-10
KLX02	336.42	334.92	337.92	3	9.90E-12	2.97E-11
KLX02	339.42	337.92	340.92	3	2.78E-07	8.34E-07

Table A5. Number of natural fractures for 1 and 3 meter sections (includes natural_sum and crush_sum), 206-341 m for KLX02.

Borehole	Sec up	Sec low					No. of fractures / 3 m	Sec up	Sec low
KLX02	206	207	0	0	0	0			
KLX02	207	208	0	0	0	0			
KLX02	208	209	3	0	3	3	3	206	209
KLX02	209	210	0	0	0	0			
KLX02	210	211	1	0	1	1			
KLX02	211	212	2	0	2	2	3	209	212
KLX02	212	213	2	0	2	2			
KLX02	213	214	1	0	1	1			
KLX02	214	215	3	0	3	3	6	212	215
KLX02	215	216	0	0	0	0			
KLX02	216	217	1	0	1	1			
KLX02	217	218	2	0	2	2	3	215	218
KLX02	218	219	4	0	4	4			
KLX02	219	220	10	0	10	10			
KLX02	220	221	1	0	1	1	15	218	221
KLX02	221	222	1	0	1	1			
KLX02	222	223	0	0	0	0			
KLX02	223	224	3	0	3	3	4	221	224
KLX02	224	225	1	0	1	1			
KLX02	225	226	2	0	2	2			
KLX02	226	227	2	0	2	2	5	224	227
KLX02	227	228	3	0	3	3			
KLX02	228	229	3	0	3	3			
KLX02	229	230	3	0	3	3	9	227	230
KLX02	230	231	3	0	3	3			
KLX02	231	232	5	0	5	5			
KLX02	232	233	3	0	3	3	11	230	233
KLX02	233	234	4	0	4	4			
KLX02	234	235	0	0	0	0			
KLX02	235	236	0	0	0	0	4	233	236
KLX02	236	237	0	0	0	0			
KLX02	237	238	0	9	9	9			
KLX02	238	239	1	0	1	1	10	236	239
KLX02	239	240	0	0	0	0			
KLX02	240	241	1	0	1	1			
KLX02	241	242	2	0	2	2	3	239	242
KLX02	242	243	3	0	3	3			
KLX02	243	244	6	0	6	6			
KLX02	244	245	2	0	2	2	11	242	245
KLX02	245	246	2	0	2	2			
KLX02	246	247	4	0	4	4			
KLX02	247	248	3	0	3	3	9	245	248
KLX02	248	249	3	0	3	3			
KLX02	249	250	5	0	5	5			
KLX02	250	251	2	0	2	2	10	248	251
KLX02	251	252	1	0	1	1			
KLX02	252	253	1	11	12	12			
KLX02	253	254	2	0	2	2	15	251	254
KLX02	254	255	8	0	8	8			
KLX02	255	256	5	0	5	5			
KLX02	256	257	1	0	1	1	14	254	257
KLX02	257	258	0	0	0	0			
KLX02	258	259	2	0	2	2			
KLX02	259	260	1	0	1	1	3	257	260
KLX02	260	261	2	0	2	2			
KLX02	261	262	2	0	2	2			
KLX02	262	263	1	0	1	1	5	260	263
KLX02	263	264	1	0	1	1			
KLX02	264	265	0	0	0	0			
KLX02	265	266	2	0	2	2	3	263	266
KLX02	266	267	5	0	5	5			
KLX02	267	268	5	0	5	5			
KLX02	268	269	6	3	9	9	19	266	269
KLX02	269	270	0	2	2	2			
KLX02	270	271	5	0	5	5			
KLX02	271	272	0	0	0	0	7	269	272
KLX02	272	273	0	0	0	0			
KLX02	273	274	0	0	0	0			
KLX02	274	275	0	0	0	0	0	272	275
KLX02	275	276	0	0	0	0			
KLX02	276	277	1	0	1	1			
KLX02	277	278	2	0	2	2	3	275	278

Borehole	Sec up	Sec low					No. of fractures / 3 m	Sec up	Sec low
KLX02	278	279	1	0	1	1			
KLX02	279	280	1	0	1	1			
KLX02	280	281	1	0	1	1	3	278	281
KLX02	281	282	0	0	0	0			
KLX02	282	283	0	0	0	0			
KLX02	283	284	3	0	3	3	3	281	284
KLX02	284	285	0	0	0	0			
KLX02	285	286	0	0	0	0			
KLX02	286	287	2	0	2	2	2	284	287
KLX02	287	288	1	0	1	1			
KLX02	288	289	0	0	0	0			
KLX02	289	290	0	0	0	0	1	287	290
KLX02	290	291	0	0	0	0			
KLX02	291	292	2	0	2	2			
KLX02	292	293	1	0	1	1	3	290	293
KLX02	293	294	2	0	2	2			
KLX02	294	295	4	0	4	4			
KLX02	295	296	1	0	1	1	7	293	296
KLX02	296	297	0	0	0	0			
KLX02	297	298	0	0	0	0			
KLX02	298	299	0	0	0	0	0	296	299
KLX02	299	300	1	0	1	1			
KLX02	300	301	1	0	1	1			
KLX02	301	302	0	0	0	0	2	299	302
KLX02	302	303	0	0	0	0			
KLX02	303	304	2	0	2	2			
KLX02	304	305	0	0	0	0	2	302	305
KLX02	305	306	1	0	1	1			
KLX02	306	307	0	0	0	0			
KLX02	307	308	0	0	0	0	1	305	308
KLX02	308	309	1	0	1	1			
KLX02	309	310	2	0	2	2			
KLX02	310	311	2	0	2	2	5	308	311
KLX02	311	312	2	0	2	2			
KLX02	312	313	0	0	0	0			
KLX02	313	314	1	0	1	1	3	311	314
KLX02	314	315	3	0	3	3			
KLX02	315	316	0	0	0	0			
KLX02	316	317	2	0	2	2	5	314	317
KLX02	317	318	1	0	1	1			
KLX02	318	319	0	0	0	0			
KLX02	319	320	1	0	1	1	2	317	320
KLX02	320	321	2	0	2	2			
KLX02	321	322	0	0	0	0			
KLX02	322	323	0	0	0	0	2	320	323
KLX02	323	324	1	0	1	1			
KLX02	324	325	2	0	2	2			
KLX02	325	326	0	0	0	0	3	323	326
KLX02	326	327	2	0	2	2			
KLX02	327	328	1	0	1	1			
KLX02	328	329	3	0	3	3	6	326	329
KLX02	329	330	0	0	0	0			
KLX02	330	331	1	0	1	1			
KLX02	331	332	1	0	1	1	2	329	332
KLX02	332	333	1	0	1	1			
KLX02	333	334	0	0	0	0			
KLX02	334	335	1	0	1	1	2	332	335
KLX02	335	336	2	0	2	2			
KLX02	336	337	0	0	0	0			
KLX02	337	338	3	0	3	3	5	335	338
KLX02	338	339	7	0	7	7			
KLX02	339	340	3	10	13	13			
KLX02	340	341	0	0	0	0	20	338	341

Table A6. Depth, flow rate and transmissivity of interpreted flowing fractures together with depths with major changes of the base-flow level (Qmin), measurements performed in the interval 200-400 m using Posiva Flowlogg. Flowing fractures within brackets are below measurement limit and thus uncertain. Overlapping flow logging, Campaign 2, see /Rouhiainen, 2000; Ludvigson et al, 2002; Carlsten et al, 2001/, L: 0.5, dL: 0.1, s: 22 m.

Depth (m)	Q (s=22m) (mL/h)	T(0-22m) (m2/s)	Baseflow (mL/h)
212	2964	3.60E-08	
213.3	158662	1.90E-06	
214	16757	2.00E-07	
215.2	5031	6.10E-08	
216.7	302	3.60E-09	
220.7	572	6.80E-09	
224.4	12542	1.50E-07	
224.9	1823	2.20E-08	
226	6625	7.90E-08	
227.7	30680	3.70E-07	
231.9	778	9.20E-09	
232.4	38	-	
233.9	5337	6.40E-08	
234.2	166	2.00E-09	
237.8	359	4.30E-09	
238	86	-	
239.1	604	7.20E-09	
241.4	990	1.20E-08	
242.3	121	-	
243.3	2870	3.50E-08	
243.8	714	8.50E-09	
244.9	733	8.70E-09	
246.7	22150	2.70E-07	
248.6	15479	1.90E-07	
249.2	1623	2.00E-08	
250.1	578	6.90E-09	
251.3	**458764**	**5.50E-06**	**20-100**
251.6	111455	1.40E-06	
252.9	41867	5.00E-07	
254.1	1269	1.60E-08	
268	16905	2.10E-07	
269	213	2.50E-09	
269.7	7977	9.70E-08	
271.1	36168	4.40E-07	
273.8	715	8.50E-09	
(275	0	-)	
276.9	462	5.50E-09	
290.5	796	9.50E-09	
292.6	219	2.60E-09	
295.1	30324	3.60E-07	
295.6	4393	5.20E-08	
298.3	698	8.30E-09	
300.6	801	9.50E-09	
(307.9	0	-)	
(310.5	0	-)	
(314.7	0	-)	
317.1	**452519**	**5.50E-06**	**100-300**
(325.4	0	-)	
(327.8	0	-)	
(328.6	0	-)	
(329.2	0	-)	
(332.7	0	-)	
337.9	9576	1.20E-07	
338.9	12983	1.70E-07	
339.1	**34185**	**4.20E-07**	**300-500**
339.6	7170	1.00E-08	
377.2	0	-)	
383.5	0	-)	
385.4	**15000**	**-**	**500-20**
389.3	375	4.50E-09	

Table A7. Transmissivities within 3 m sections based on Table A6, 206-341 m.

Sec up	Sec low	T (Posiva) (m2/s)	T (Posiva) (m2/s)	T (Posiva) (m2/s)
206	209			
209	212			
212	215	1.9E-06	2E-07	3.6E-08
215	218	6.1E-08	3.6E-09	
218	221	6.8E-09		
221	224			
224	227	1.5E-07	2.2E-08	7.9E-08
227	230	3.7E-07		
230	233	9.2E-09		
233	236	6.4E-08	2E-09	
236	239	4.3E-09		
239	242	7.2E-09	1.2E-08	
242	245	3.5E-08	8.5E-09	8.7E-09
245	248	2.7E-07		
248	251	1.9E-07	2E-08	6.9E-09
251	254	5.5E-06	1.4E-06	5E-07
254	257	1.6E-08		
257	260			
260	263			
263	266			
266	269	2.1E-07	2.5E-09	
269	272	9.7E-08	4.4E-07	
272	275	8.5E-09		
275	278	5.5E-09		
278	281			
281	284			
284	287			
287	290			
290	293	9.5E-09	2.6E-09	
293	296	3.6E-07	5.2E-08	
296	299	8.3E-09		
299	302	9.5E-09		
302	305			
305	308			
308	311			
311	314			
314	317			
317	320	5.5E-06		
320	323			
323	326			
326	329			
329	332			
332	335			
335	338	1.2E-07		
338	341	1.7E-07	4.2E-07	1E-08

Table A8. Estimated transmissivities within 3 m sections using non-parametric method (M1), 206-341 m compared to transmissivities of conductive features based on Posiva Flowlogg (Table A6-A7).

Sec up	Sec low	No. of fractures	Transmissivity [m2/s] Estimated	Identified
206	209	3	7.5E-13	
			1.2E-11	
			3.1E-09	
209	212	3	8.0E-13	
			1.3E-11	
			7.9E-09	
212	215	6	2.2E-13	
			2.5E-13	
			8.0E-13	
			8.7E-12	3.6E-08
			8.5E-11	2E-07
			2.7E-06	1.9E-06
215	218	3	5.6E-13	
			1.7E-11	3.6E-09
			6.4E-08	6.1E-08
218	221	15	6.0E-12	
			1.1E-11	
			1.1E-11	
			1.1E-11	
			1.1E-11	
			1.2E-11	
			3.7E-11	
			3.9E-11	
			4.2E-11	
			1.6E-10	
			2.4E-10	
			4.3E-10	
			4.6E-10	
			1.2E-09	
			4.3E-09	6.8E-09
221	224	4	4.3E-12	
			1.5E-11	
			1.7E-10	
			2.7E-09	
224	227	5	1.4E-12	
			4.7E-12	
			2.4E-11	2.2E-08
			9.7E-11	7.9E-08
			2.9E-07	1.5E-07
227	230	9	2.3E-12	
			2.4E-12	
			2.6E-12	
			8.3E-12	
			9.8E-12	
			9.0E-11	
			1.6E-10	
			1.3E-09	
			4.1E-07	3.7E-07
230	233	11	5.6E-12	
			8.0E-12	
			8.0E-12	
			8.9E-12	
			2.7E-11	
			2.8E-11	
			1.1E-10	
			3.1E-10	
			3.2E-10	
			2.9E-09	
			5.0E-09	9.2E-09

Sec up	Sec low	No. of fractures	Transmissivity [m2/s] Estimated	Identified
233	236	4	1.7E-12	
			6.1E-12	
			6.8E-11	2E-09
			3.4E-08	6.4E-08
236	239	10	6.1E-12	
			8.7E-12	
			8.7E-12	
			9.8E-12	
			3.0E-11	
			3.3E-11	
			1.5E-10	
			3.4E-10	
			6.0E-10	
			3.4E-09	4.3E-09
239	242	3	1.1E-12	
			2.3E-11	7.2E-09
			1.8E-08	1.2E-08
242	245	11	1.8E-12	
			2.6E-12	
			2.6E-12	
			3.0E-12	
			9.2E-12	
			9.5E-12	
			4.5E-11	
			1.0E-10	
			1.8E-10	8.5E-09
			1.0E-09	8.7E-09
			1.6E-08	3.5E-08
245	248	9	1.6E-12	
			1.6E-12	
			1.8E-12	
			5.7E-12	
			6.8E-12	
			5.7E-11	
			1.1E-10	
			6.4E-10	
			2.1E-07	2.7E-07
248	251	10	2.2E-12	
			2.2E-12	
			2.3E-12	
			7.5E-12	
			7.8E-12	
			3.8E-11	
			8.7E-11	
			1.5E-10	6.9E-09
			1.2E-09	2E-08
			2.8E-07	1.9E-07
251	254	15	5.9E-13	
			1.1E-12	
			1.1E-12	
			1.1E-12	
			1.2E-12	
			3.7E-12	
			3.8E-12	
			4.5E-12	
			1.9E-11	
			4.3E-11	
			4.3E-11	
			1.2E-10	
			5.8E-10	5E-07
			1.9E-08	1.4E-06
			1.9E-05	5.5E-06

Sec up	Sec low	No. of fractures	Transmissivity [m2/s] Estimated	Identified
254	257	14	5.4E-12	
			1.0E-11	
			1.0E-11	
			1.0E-11	
			1.1E-11	
			3.4E-11	
			3.5E-11	
			4.0E-11	
			1.7E-10	
			3.8E-10	
			3.9E-10	
			7.0E-10	
			3.9E-09	
			6.5E-09	1.6E-08
257	260	3	6.3E-12	
			1.2E-11	
			1.2E-11	
260	263	5	5.1E-12	
			6.2E-12	
			6.2E-12	
			6.2E-12	
			6.2E-12	
263	266	3	6.3E-12	
			1.2E-11	
			1.2E-11	
266	269	19	1.3E-12	
			2.4E-12	
			2.4E-12	
			2.4E-12	
			2.4E-12	
			2.5E-12	
			2.7E-12	
			8.0E-12	
			8.3E-12	
			8.7E-12	
			1.1E-11	
			4.1E-11	
			9.2E-11	
			9.3E-11	
			1.6E-10	
			8.6E-10	
			9.3E-10	
			1.5E-09	2.5E-09
			2.2E-07	2.1E-07
269	272	7	2.6E-12	
			2.6E-12	
			9.0E-12	
			3.6E-11	
			1.0E-10	
			1.0E-09	9.7E-08
			5.4E-07	4.4E-07
272	275	0 1	6.8E-09	8.5E-09
275	278	3	8.9E-13	
			1.5E-11	
			5.1E-09	5.5E-09
278	281	3	6.3E-12	
			1.2E-11	
			1.2E-11	
281	284	3	6.3E-12	
			1.2E-11	
			1.2E-11	

Sec up	Sec low	No. of fractures	Transmissivity [m2/s] Estimated	Identified
284	287	2	6.6E-12	
			2.3E-11	
287	290	1	8.0E-10	
290	293	3	7.8E-13	
			1.5E-11	2.6E-09
			1.3E-08	9.5E-09
293	296	7	2.3E-12	
			2.3E-12	
			8.1E-12	
			3.3E-11	
			9.1E-11	
			9.0E-10	5.2E-08
			4.9E-07	3.6E-07
296	299	0 1	6.5E-08	8.3E-09
299	302	2	1.5E-12	
			7.6E-09	9.5E-09
302	305	2	6.6E-12	
			2.3E-11	
305	308	1	4.5E-10	
308	311	5	5.6E-12	
			6.3E-12	
			2.3E-11	
			2.2E-10	
			3.1E-09	
311	314	3	6.9E-12	
			2.4E-11	
			2.7E-10	
314	317	5	3.3E-12	
			3.7E-12	
			1.2E-11	
			1.3E-10	
			1.2E-09	
317	320	2	4.1E-13	
			5.4E-06	5.5E-06
320	323	2	6.6E-12	
			2.3E-11	
323	326	3	3.6E-12	
			6.0E-11	
			2.2E-09	
326	329	6	3.2E-12	
			3.4E-12	
			1.1E-11	
			5.5E-11	
			2.2E-10	
			5.4E-09	
329	332	2	1.8E-12	
			3.1E-09	
332	335	2	7.0E-12	
			7.8E-10	
335	338	5	5.1E-12	
			6.2E-12	
			6.2E-12	
			6.2E-12	
			6.2E-12	1.2E-07
338	341	20	2.5E-12	
			4.5E-12	
			4.6E-12	
			4.6E-12	
			4.6E-12	
			4.7E-12	
			5.2E-12	
			1.5E-11	
			1.6E-11	
			1.6E-11	
			1.9E-11	
			7.9E-11	
			1.2E-10	
			1.8E-10	
			1.8E-10	
			3.2E-10	
			1.7E-09	
			2.5E-09	1E-08
			3.9E-08	1.7E-07
			7.9E-07	4.2E-07
		254 256	3.1E-05	1.83E-05

38

Data for study of inflow and orientation of conductive features (KA3376B01)

Table B1. KA3376B01: Approximate inflow (Q) and location of in flow along borehole (L) (measured during drilling). 3 m sections with measured inflow marked with frames.

Drill length (m)	Sub Start Date	Sub Stop Date	Drill length (m)	Acc. Inflow drilling (L/min)		d Inflow drilling (L/min)
1.68	2002-11-08 15:22	2002-11-08 15:48	1.68	0		
2.28	2002-11-08 15:53	2002-11-08 16:12	2.28	0		
2.28	2002-11-10 08:57	2002-11-10 09:03	2.28	0		
3.65	2002-11-10 09:18	2002-11-10 09:29	3.65	0		
5.1	2002-11-10 09:42	2002-11-10 09:54	5.1	0		
6.35	2002-11-10 10:03	2002-11-10 10:12	6.35	0		
7.83	2002-11-10 10:28	2002-11-10 10:43	7.83	0		
9.3	2002-11-10 11:01	2002-11-10 11:22	9.3	0		
10.5	2002-11-10 13:23	2002-11-10 13:30	10.5	0		
11.95	2002-11-10 13:48	2002-11-10 14:02	11.95	0		
13.39	2002-11-10 14:09	2002-11-10 14:18	13.39	0		
14.87	2002-11-10 14:29	2002-11-10 14:39	14.87	0		
16.32	2002-11-10 14:49	2002-11-10 15:05	16.32	0		
17.25	2002-11-10 15:36	2002-11-10 15:46	17.25	0		
18.83	2002-11-10 16:20	2002-11-10 16:29	18.83	0		
19.38	2002-11-10 16:57	2002-11-10 17:06	19.38	0		
20.9	2002-11-10 17:31	2002-11-10 17:38	20.9	0		
21.78	2002-11-11 07:52	2002-11-11 07:57	21.78	0		
23.23	2002-11-11 08:12	2002-11-11 08:21	23.23	0		
24.69	2002-11-11 08:43	2002-11-11 08:52	24.69	0		
26.15	2002-11-11 09:14	2002-11-11 09:26	26.15	0		
27.61	2002-11-11 09:42	2002-11-11 09:50	27.61	0		
29.13	2002-11-11 10:14	2002-11-11 10:24	29.13	0		
30.6	2002-11-11 10:37	2002-11-11 10:47	30.6	0		
32.06	2002-11-11 11:01	2002-11-11 11:09	32.06	0		
33.52	2002-11-11 12:47	2002-11-11 12:59	33.52	0		
34.97	2002-11-11 13:11	2002-11-11 13:21	34.97	0		
36.44	2002-11-11 13:39	2002-11-11 13:48	36.44	0		
37.82	2002-11-11 14:12	2002-11-11 14:20	37.82	0		
39.32	2002-11-11 14:37	2002-11-11 14:46	39.32	0		
40.76	2002-11-11 15:22	2002-11-11 15:29	40.76	0		
42.23	2002-11-11 15:46	2002-11-11 15:53	42.23	0		
43.67	2002-11-11 16:28	2002-11-11 16:34	43.67	0		
45.17	2002-11-11 16:49	2002-11-11 16:59	45.17	0	45-48 m	
45.57	2002-11-18 15:47	2002-11-18 15:50	45.57	0		
45.87	2002-11-18 15:07	2002-11-18 15:13	45.87	0		
46.06	2002-11-18 16:38	2002-11-18 16:42	46.06	0		
46.23	2002-11-19 09:03	2002-11-19 09:14	46.23	0		
46.31	2002-11-19 10:55	2002-11-19 10:58	46.31	0		
46.84	2002-11-19 10:01	2002-11-19 10:08	46.84	0		
47.01	2002-11-20 08:40	2002-11-20 08:53	47.01	0		
47.68	2002-11-20 09:38	2002-11-20 09:48	47.68	5.8		5.8
48.18	2002-11-20 10:53	2002-11-20 11:01	48.18	16	48-51 m	
48.88	2002-11-20 12:45	2002-11-20 12:49	48.88	16		
49.89	2002-11-20 13:14	2002-11-20 13:22	49.89	28		
50	2002-11-20 14:44	2002-11-20 14:48	50	55		
50.56	2002-11-20 13:56	2002-11-20 14:02	50.56	55		
50.72	2002-11-21 08:27	2002-11-21 08:43	50.72	55		
50.82	2002-11-21 14:51	2002-11-21 14:57	50.82	55		49.2
51.38	2002-11-21 16:22	2002-11-21 16:28	51.38	55	51-54 m	
51.54	2002-11-22 08:45	2002-11-22 09:03	51.54	55		
52.21	2002-11-22 11:11	2002-11-22 11:28	52.21	55		
52.34	2002-11-22 13:17	2002-11-22 13:28	52.34	66		
52.96	2002-11-22 14:03	2002-11-22 14:14	52.96	66		
53.14	2002-11-23 08:36	2002-11-23 08:50	53.14	66		
53.82	2002-11-23 09:37	2002-11-23 09:48	53.82	66		11

54.15	2002-11-23 10:40	2002-11-23 10:47	54.15	66	
54.82	2002-11-23 11:11	2002-11-23 11:23	54.82	66	
55.18	2002-11-23 11:49	2002-11-23 11:55	55.18	66	
55.84	2002-11-23 12:23	2002-11-23 12:36	55.84	66	
55.99	2002-11-24 08:18	2002-11-24 08:33	55.99	66	
56.66	2002-11-24 09:24	2002-11-24 09:35	56.66	66	
56.81	2002-11-24 10:32	2002-11-24 10:39	56.81	66	
57.4	2002-11-24 12:27	2002-11-24 12:38	57.4	66	57-60 m
57.61	2002-11-24 13:07	2002-11-24 13:13	57.61	66	
58.28	2002-11-24 13:39	2002-11-24 13:53	58.28	75	
58.41	2002-11-25 08:07	2002-11-25 08:23	58.41	75	
58.46	2002-11-25 09:37	2002-11-25 09:39	58.46	75	
59.11	2002-11-25 10:11	2002-11-25 10:22	59.11	75	
59.41	2002-11-25 10:58	2002-11-25 11:16	59.41	75	9
60.81	2002-11-25 13:21	2002-11-25 13:34	60.81	75	
62.28	2002-11-25 13:56	2002-11-25 14:11	62.28	75	
63.5	2002-11-25 14:51	2002-11-25 15:29	63.5	80	63-66 m
63.67	2002-11-25 16:17	2002-11-25 16:22	63.67	80	
65.08	2002-11-25 16:50	2002-11-25 17:02	65.08	80	5
66.52	2002-11-25 17:25	2002-11-25 17:35	66.52	80	
67.82	2002-11-25 18:04	2002-11-25 18:17	67.82	80	
69.27	2002-11-26 08:03	2002-11-26 08:13	69.27	80	
70.75	2002-11-26 08:38	2002-11-26 08:51	70.75	80	
72.2	2002-11-26 09:43	2002-11-26 09:52	72.2	80	
73.64	2002-11-26 10:17	2002-11-26 10:36	73.64	80	
75.1	2002-10-26 10:59	2002-11-26 11:13	75.1	80	
76.55	2002-11-26 13:09	2002-11-26 13:24	76.55	80	
77.84	2002-11-26 13:47	2002-11-26 14:03	77.84	80	
79.28	2002-11-26 14:36	2002-11-26 14:51	79.28	80	
80.19	2002-11-26 15:28	2002-11-26 15:39	80.19	80	
					80

KA3376B01
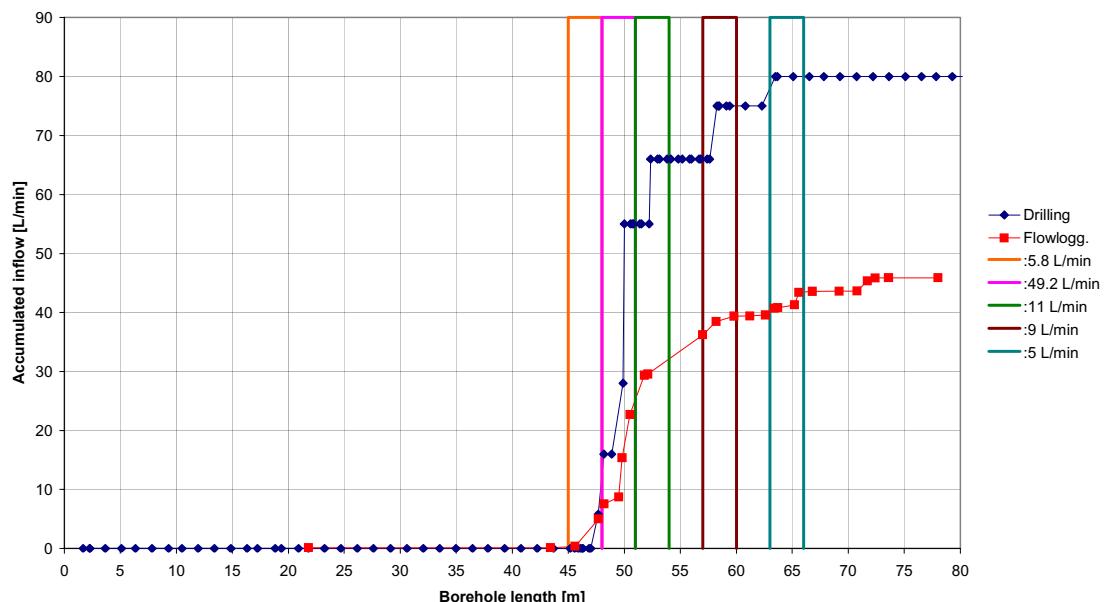
Figure B1. Accumulated inflow during drilling and based on Posiva Flowlogg (data below, measurement limit approx. 5 L/min)

Table B2. Inflow based on Posiva Flowlogg (measurement limit approx. 5 L/min).

Depth (m)	Inflow (mL/h)	Inflow Posiva (L/min)	
21.8	6800	0.11	0.11
43.4	1300	0.02	0.14
45.6	14000	0.23	0.37
47.7	280000	4.67	5.04
48.2	150000	2.50	7.54
49.5	70000	1.17	8.70
49.8	400000	6.67	15.37
50.5	440000	7.33	22.70
51.8	400000	6.67	29.37
52.1	12000	0.20	29.57
57	400000	6.67	36.24
58.2	134000	2.23	38.47
59.8	54000	0.90	39.37
61.2	2000	0.03	39.40
62.6	9800	0.16	39.57
63.4	68000	1.13	40.70
63.7	7000	0.12	40.82
65.2	30000	0.50	41.32
65.6	126000	2.10	43.42
66.8	9000	0.15	43.57
69.2	2800	0.05	43.61
70.8	1400	0.02	43.64
71.7	105000	1.75	45.39
72.4	29000	0.48	45.87
73.6	920	0.02	45.88

***Table B3. Strike, dip and location along borehole (L) for natural fractures
(from BIPS and core mapping). Division into 3 m sections shaded. 3 m sections
with inflow marked with frames.***

Idcode	From Length (m)	To Length (m)	Sec up (m)	Sec low (m)	No. Natural fr.	Strike (degr.)	Dip (degr.)	Inflow drilling
KA3376B01	3.29	3.29	3	6	6	270.0	4.6	
KA3376B01	3.74	3.74				104.0	5.0	
KA3376B01	3.91	3.91				90.0	4.5	
KA3376B01	3.97	3.97				310.0	17.3	
KA3376B01	4.20	4.20				311.0	7.1	
KA3376B01	5.92	5.92				102.0	13.7	
KA3376B01	6.01	6.01	6	9	7	106.0	4.8	
KA3376B01	6.11	6.11				271.0	5.0	
KA3376B01	7.23	7.23				276.0	11.9	
KA3376B01	8.07	8.07				274.0	10.0	
KA3376B01	8.36	8.36				160.0	24.2	
KA3376B01	8.79	8.79				314.0	4.6	
KA3376B01	8.81	8.81				68.0	4.1	
KA3376B01	10.22	10.22	9	12	3	270.0	6.2	
KA3376B01	10.57	10.57				30.0	40.3	
KA3376B01	11.87	11.87				98.0	4.6	
KA3376B01	12.80	12.80	12	15	5	100.0	16.0	
KA3376B01	13.55	13.55				353.0	33.4	
KA3376B01	13.87	13.87				83.0	4.7	
KA3376B01	13.94	13.94				307.0	4.7	
KA3376B01	14.81	14.81				333.0	66.5	
KA3376B01	15.02	15.02	15	18	8	113.0	55.8	
KA3376B01	15.83	15.83				31.0	24.1	
KA3376B01	15.88	15.88				122.0	74.3	
KA3376B01	16.29	16.29				150.0	82.8	
KA3376B01	16.48	16.48				189.0	28.9	
KA3376B01	16.51	16.51				274.0	9.2	
KA3376B01	17.10	17.10				102.0	43.5	
KA3376B01	17.81	17.81				122.0	20.7	
KA3376B01	18.20	18.20	18	21	2	90.0	7.9	
KA3376B01	20.26	20.26				97.0	5.2	
KA3376B01	21.34	21.34	21	24	9	332.0	55.4	
KA3376B01	21.62	21.62				342.0	24.4	
KA3376B01	21.64	21.64				354.0	27.2	
KA3376B01	21.72	21.72				107.0	16.7	
KA3376B01	21.73	21.73				92.0	23.0	
KA3376B01	21.77	21.77				89.0	6.2	
KA3376B01	21.87	21.87				24.0	12.3	
KA3376B01	22.27	22.27				91.0	14.1	
KA3376B01	23.36	23.36				271.0	17.6	
KA3376B01	24.90	24.90	24	27	5	104.0	40.1	
KA3376B01	25.48	25.48				268.0	14.3	
KA3376B01	25.77	25.77				163.0	50.6	
KA3376B01	26.32	26.32				289.0	13.6	
KA3376B01	26.58	26.58				87.0	57.7	
KA3376B01	27.78	27.78	27	30	4	67.0	29.6	
KA3376B01	28.25	28.25				270.0	1.8	
KA3376B01	28.26	28.26				271.0	2.3	
KA3376B01	28.41	28.41				92.0	30.7	
KA3376B01	30.00	30.00	30	33	3	270.0	3.9	
KA3376B01	30.32	30.32				271.0	6.1	
KA3376B01	30.35	30.35				272.0	3.1	
KA3376B01	33.15	33.15	33	36	5	270.0	6.3	
KA3376B01	34.39	34.39				91.0	6.0	
KA3376B01	34.53	34.53				92.0	3.1	
KA3376B01	34.91	34.91				31.0	45.4	
KA3376B01	35.95	35.95				270.0	3.7	
KA3376B01	38.12	38.12	36	39	3	163.0	63.5	
KA3376B01	38.48	38.48				148.0	22.7	
KA3376B01	38.85	38.85				141.0	51.4	
KA3376B01	39.02	39.02	39	42	6	105.0	48.3	
KA3376B01	39.40	39.40				132.0	37.8	
KA3376B01	39.55	39.55				107.0	42.8	
KA3376B01	40.34	40.34				93.0	4.0	
KA3376B01	41.31	41.31				93.0	12.2	
KA3376B01	41.91	41.91				278.0	10.7	

KA3376B01	43.11	43.11	42	45	11	301.0	23.1	
KA3376B01	43.17	43.17				272.0	7.5	
KA3376B01	43.21	43.21				264.0	19.2	
KA3376B01	43.24	43.24				209.0	22.7	
KA3376B01	43.27	43.27				228.0	19.1	
KA3376B01	43.41	43.41				271.0	10.4	
KA3376B01	43.47	43.47				271.0	6.5	
KA3376B01	43.52	43.52				113.0	8.3	
KA3376B01	43.66	43.66				279.0	2.0	
KA3376B01	43.95	43.95				89.0	4.5	
KA3376B01	43.96	43.96				89.0	3.6	
KA3376B01	47.18	47.18	45	48	5	9.4	64.5	5.8
KA3376B01	47.50	47.50				149.4	82.4	
KA3376B01	47.66	47.66				138.0	82.7	
KA3376B01	47.74	47.74				135.3	82.8	
KA3376B01	47.85	47.85				19.2	51.3	
KA3376B01	48.05	48.05	48	51	7	316.3	75.6	49.2
KA3376B01	48.08	48.08				299.7	74.5	
KA3376B01	48.27	48.27				33.6	64.6	
KA3376B01	48.35	48.35				297.7	88.1	
KA3376B01	48.72	48.72				328.0	79.0	
KA3376B01	48.83	48.83				148.6	81.7	
KA3376B01	50.42	50.42				125.7	85.8	
KA3376B01	51.20	51.20	51	54	4	132.4	79.6	11
KA3376B01	51.69	51.69				129.6	69.3	
KA3376B01	51.78	51.78				123.2	70.4	
KA3376B01	51.99	51.99				4.1	75.3	
KA3376B01	54.32	54.32	54	57	3	105.4	80.5	
KA3376B01	56.92	56.92				135.5	82.8	
KA3376B01	57.00	57.00				130.7	78.4	
KA3376B01	57.87	57.87	57	60	5	109.3	87.9	9
KA3376B01	58.09	58.09				135.5	65.7	
KA3376B01	59.14	59.14				169.7	89.3	
KA3376B01	59.66	59.66				149.7	63.6	
KA3376B01	59.69	59.69				153.5	77.8	
KA3376B01	60.42	60.42	60	63	7	292.1	48.7	
KA3376B01	61.07	61.07				134.5	85.3	
KA3376B01	61.10	61.10				124.6	76.0	
KA3376B01	62.23	62.23				116.0	74.6	
KA3376B01	62.36	62.36				316.8	83.3	
KA3376B01	62.50	62.50				313.5	82.1	
KA3376B01	62.57	62.57				313.3	80.4	
KA3376B01	63.20	63.20	63	66	18	355.8	45.5	5
KA3376B01	63.23	63.23				321.6	56.8	
KA3376B01	63.25	63.25				311.1	49.3	
KA3376B01	63.47	63.47				135.5	81.5	
KA3376B01	63.51	63.51				136.1	77.5	
KA3376B01	63.54	63.54				317.5	88.2	
KA3376B01	63.61	63.61				353.0	70.6	
KA3376B01	63.64	63.64				349.7	86.8	
KA3376B01	63.75	63.75				357.1	79.9	
KA3376B01	63.76	63.76				107.3	80.5	
KA3376B01	63.79	63.79				123.2	71.7	
KA3376B01	64.51	64.51				272.3	78.8	
KA3376B01	65.15	65.15				160.3	82.3	
KA3376B01	65.30	65.30				315.5	48.7	
KA3376B01	65.35	65.35				326.2	80.0	
KA3376B01	65.48	65.48				141.5	86.2	
KA3376B01	65.51	65.51				318.7	43.8	
KA3376B01	65.56	65.56				358.4	80.3	

KA3376B01	66.24	66.24	66	69	7	342.9	49.6
KA3376B01	66.47	66.47				297.0	87.3
KA3376B01	67.80	67.80				294.7	84.6
KA3376B01	67.89	67.89				113.4	88.4
KA3376B01	68.22	68.22				330.7	67.2
KA3376B01	68.27	68.27				332.6	67.9
KA3376B01	68.99	68.99				329.1	62.9
KA3376B01	69.01	69.01	69	72	9	344.0	64.3
KA3376B01	69.21	69.21				317.4	84.2
KA3376B01	69.26	69.26				328.8	77.0
KA3376B01	69.72	69.72				339.2	57.9
KA3376B01	69.76	69.76				348.8	46.8
KA3376B01	70.00	70.00				323.2	70.6
KA3376B01	70.95	70.95				353.4	58.1
KA3376B01	71.45	71.45				316.0	77.2
KA3376B01	71.60	71.60				322.7	76.4
KA3376B01	72.38	72.38	72	75	5	294.2	80.8
KA3376B01	72.68	72.68				352.9	88.3
KA3376B01	73.59	73.59				346.9	52.8
KA3376B01	74.41	74.41				8.0	62.3
KA3376B01	74.85	74.85				332.8	74.8
KA3376B01	75.92	75.92	75	78	2	317.0	78.9
KA3376B01	76.58	76.58				156.4	84.1
					149		